SANDIA REPORT

SAND2007-3316
Unlimited Release
Printed June 2007

Wetting and Free Surface Flow Modeling for Potting and Encapsulation

Lisa Mondy, Rekha Rao, Carlton Brooks, David Noble, Richard Givler, Amy Sun, Andrew Kraynik, Thomas Baer, Edward Wilkes, Patrick Notz, Matthew Hopkins, Anne Grillet, Ray O. Cote, Jaime N. Castañeda, Doug Adolf, Jim Mahoney, Kathryn Berchtold, Michael Brooks, and Alan Graham.

Prepared by
Sandia National Laboratories
Albuquerque, New Mexico 87185 and Livermore, California 94550

Sandia is a multiprogram laboratory operated by Sandia Corporation,
a Lockheed Martin Company, for the United States Department of Energy's
National Nuclear Security Administration under Contract DE-AC04-94AL85000.

Sandia National Laboratories

Issued by Sandia National Laboratories, operated for the United States Department of Energy by Sandia Corporation.

Printed in the United States of America. This report has been reproduced directly from the best available copy.

Available to DOE and DOE contractors from
U.S. Department of Energy
Office of Scientific and Technical Information
P.O. Box 62
Oak Ridge, TN 37831

Telephone: (865)576-8401
Facsimile: (865)576-5728
E-Mail: reports@adonis.osti.gov
Online ordering: http://www.osti.gov/bridge

Available to the public from
U.S. Department of Commerce
National Technical Information Service
5285 Port Royal Rd
Springfield, VA 22161

Telephone: (800)553-6847
Facsimile: (703)605-6900
E-Mail: orders@ntis.fedworld.gov
Online order: http://www.ntis.gov/help/ordermethods.asp?loc=7-4-0#online

SAND2007-3316
Unlimited Release
Printed June 2007

Wetting and Free Surface Flow Modeling for Potting and Encapsulation

Lisa Mondy, Rekha Rao, Carlton Brooks, David Noble, Richard Givler, Amy Sun, Andrew Kraynik, Thomas Baer, Edward Wilkes, Patrick Notz, Matthew Hopkins, Anne Grillet, Ray O. Cote, Jaime N. Castañeda, Doug Adolf

Sandia National Laboratories
P.O. Box 5800
Albuquerque, NM 87185-0836

Jim Mahoney

Kansas City Plant
P.O. Box 419159
Kansas City, MO 64141-6159

Kathryn Berchtold, Michael Brooks, and Alan Graham

Los Alamos National Laboratories
P.O. Box 1663
Los Alamos, NM 87545

Abstract

As part of an effort to reduce costs and improve quality control in encapsulation and potting processes the Technology Initiative Project "Defect Free Manufacturing and Assembly" has completed a computational modeling study of flows representative of those seen in these processes. Flow solutions are obtained using a coupled, finite-element based, numerical method based on the GOMA/ARIA suite of Sandia flow solvers. The evolution of the free surface is solved with an advanced level set algorithm. This approach incorporates novel methods for representing surface tension and wetting forces that affect the evolution of the free surface. In addition, two commercially available codes, ProCAST and MOLDFLOW, are also used on geometries representing encapsulation processes at the Kansas City Plant. Visual observations of the flow in several geometries are recorded in the laboratory and compared to the models. Wetting properties for the materials in these experiments are measured using a unique flow-through goniometer.

Acknowledgments

The authors would like to acknowledge Tom Grasser for help in creating the experimental molds and Brian Rutherford for help in analyzing the sensitivity studies. We would also like to thank our reviewers Jeremy Lechman and Chris Bourdon for their timely and helpful comments.

Contents

Figures

Tables

1. Introduction

In many manufacturing processes, control of liquid flow in a complex geometry is required to ensure a consistent product. Under undesirable process conditions, incomplete wetting leaves entrapped air bubbles. This is especially important to avoid during encapsulation and potting of certain electronics and weapon components. Here, a liquid potting material, for example, an epoxy or a silicone, is injected around the components to be encapsulated, after which the liquid cures to a solid material that performs various functions depending on the product. These functions can include holding parts in place and protecting from shock and vibration. Usually, encapsulation is almost the last step in the manufacturing process, and poor quality control in this final step can cause the entire part to be scrapped or an expensive procedure to remove the potting material and repeat the step. To avoid expensive build-and-test cycles, it is desirable to use computational modeling in the process design and optimization stages to mitigate the possibility of air entrapment. In addition, even a "first strike tool" can be used to yield valuable information much earlier in the design and production process. This information includes (but is not limited to):

- Volume estimates of cavities
- Mold construction strategies
- Fill locations
- Number of fill locations
- Orientation (for filling and curing)

Here we explore the use of three codes to model various scenarios and validate the calculations with experimental results.

The first two codes tested are ARIA and GOMA, developed at Sandia National Laboratories [Schunk et al. 2002, Notz et al. 2006]. These are coupled, finite-element based, multi-physics codes that include state-of-the-art free surface and interface tracking methods. The evolution of the free surface was solved with an advanced level set algorithm. This approach incorporates novel methods for representing surface tension and wetting forces that affect the evolution of the free surface [Baer et al. 2003]. State-of-the-art models for dynamic wetting are included.

Understanding dynamic wetting has been the subject of numerous experimental and theoretical studies and is still a research topic. A key measure of relative forces during wetting is the capillary number $Ca = (\mu_{\text{liquid}} U)/\sigma$, the ratio of viscosity times the characteristic velocity to the surface tension. Even though a low *Ca* gives an indication of a flow regime that is favorable to wetting, it is insufficient to describe the dynamic wetting process. We will show that both the geometry itself and the contact angle formed by the three contacting phases can also influence the wetting behavior.

The static contact angle, defined as the angle between the wall and the liquid at static equilibrium, is a function of local molecular interactions at the contact line. Young's equation defines the relationship between static contact angle and liquid-gas, gas-solid, and liquid-solid surface tensions [Young 1805]:

$$cos\,\theta^{eq} = \frac{\sigma_{sg} - \sigma_{sl}}{\sigma_{lg}} \quad . \tag{1}$$

θ^{eq} is the equilibrium contact angle between the solid wall and liquid, σ_{sg}, σ_{sl}, and σ_{lg} are the surface tensions between the solid-gas, solid-liquid, and liquid-gas phases, respectively. Equation (1) is no longer satisfied when dynamic wetting is involved because the viscous stress deforms the meniscus during flow. Furthermore, it is known that the balance of viscous forces will cause a singularity at the contact line [Probstein 1994]. For nonzero *Ca*, the dynamic contact angle θ will therefore differ from its static value θ^{eq}. Blake [1993] noted that the advancing angle is a monotonically increasing function of *Ca*. The degree of velocity dependence will however increase steeply as viscosity increases or surface tension decreases.

To model dynamic contact for our filling process, the dynamic angle is tied to the balance of forces at the advancing wetting line, namely the tangential wetting line force, liquid-gas surface tension force, and fluid viscous force. Furthermore, we directly measure in the laboratory the dynamic contact angle as a function of the velocity of the wetting line v_{wet} for the liquids and surfaces used in our validation experiments as input to the wetting model used. This wetting model is based on a version of the Blake [1969] equation relating the wetting line speed to the wetting angles and constants v_0 and γ, where γ can represent a thermally scaled surface tension, *i.e.* $\sigma/2nkT$, or is simply another fitting parameter:

$$v_{wetting} = v_0 \sinh(\gamma(\cos\theta - \cos\theta^{eq})) \quad . \tag{2}$$

One important point worth noting is that a decrease of surface tension affects the dynamic wettability in a complex way. It is known that decreasing the surface tension (e.g. with addition of surfactant in the liquid) decreases the static contact angle, which can increase the wetting speed. However, a decrease in the surface tension will also increase the Ca, which we have shown [Sun et al. 2005] can decrease the wettability. We elaborate on this point with a sensitivity study for flow between parallel plates where one plate includes a groove. Here it becomes clear that the interplay between wall slip, dynamic contact angles, and surface tension are not captured entirely in a single dimensionless group.

As the flow geometry becomes more complex, whether or not bubbles are trapped can become almost independent of the wetting behavior, as will be shown with another sensitivity study using GOMA/ARIA. Because of this we also have explored modeling a representative encapsulation process flow using commercially available codes ProCAST and MOLDFLOW. Although neither includes the above advanced wetting models, ProCAST and MOLDFLOW can aid in the prediction of the likely areas to trap bubbles in complex geometries.

ProCAST is a commercial code licensed by the ESI Group, an international company that develops simulation software for various manufacturing processes. Although ProCAST was developed originally to simulate high speed flows of liquids with relatively low viscosities for metal casting processes, it can also be used to simulate highly viscous flow problems like those in encapsulation and potting processes. ProCAST uses a volume-of-fluid (VOF) algorithm to track the advancing fluid front through a previously tessellated region that defines the empty cavity. The fluid front is advanced within each element by solving the fluid momentum equations and, then, adjusted to satisfy mass conservation. A proprietary algorithm computes the local curvature of the advancing front by assessing the degree of fill for neighboring elements. From this information, an adjustment to the pressure field along the free surface can be computed which accounts for the effects of surface tension. An additional option allows trapped gas to offer a pressure resistance so that voids created by the flow do not necessarily disappear as flow continues.

MOLDFLOW originated from the plastics industry, moving from a strictly 2D thermoplastic injecting simulation tool of the 1980's to a comprehensive suite of codes designed for many plastic filling applications. Of merit for this project is MOLDFLOWs' capabilities to evaluate fills in 3D volumes, deriving solutions based on the Navier-Stokes set of equations. However, MOLDFLOW cannot predict the effects of high surface tension or time dependent viscosity. Because there is no effect of pressure resistance from trapped gas all areas will eventually fill in the simulations. Those areas last to fill, however, can give valuable information about the possible areas of trapped gas.

Four types of flows are studied. The first model is a representation of the flow in the goniometer. Here fluid is forced through a short tube onto a plate, where it spreads both by forced convection and spreading due to gravity. This is the geometry in which wetting parameters are determined; therefore, this example tests that the level set implementation does not interfere adversely with the wetting model. The second type of geometry represents a fluid displacing air as it flows between parallel plates where the upper plate has a notch or groove perpendicular to the flow direction. The notched portion of the upper plate is representative of a mold joint, a feature in the part to be potted, or even a long scratch in the plate surface. The third type models fluid displacing air as it enters an expansion region or cavity. The fourth is similar to the third, but here there are obstacles within the cavity that cause the flow to split and then recombine past the obstacle, creating knit lines and potentially trapping bubbles.

Experiments, in which fluids are injected into clear plastic molds that allowed video recording of the shape and movement of the entering front, are performed for all geometries reported. These laboratory observations are used to validate the codes. Both calculations in 2D approximations to the geometries as well as more complex fully 3D calculations are compared to the experimental results.

Results show that two dimensional modeling can often show qualitative trends, such as regions that are likely to trap bubbles, even if the quantitative values of bubble size are not exact. Although requiring more time and resources, 3D models can improve the quantitative predictions. Many of the trends of the experiments are captured by the level set modeling, though quantitative agreement is often lacking. We feel that the lack of agreement between the experiment and simulation probably stems from several factors, including the diffuse interface representation in the level set algorithm, the assumed high value for the gas phase viscosity necessary for numerical stability, and the wetting parameters. The wetting parameters are determined from a model and are not necessarily material properties, but instead can depend on the flow itself. Wetting is currently a research topic, and we believe that this work shows that parameters determined in one flow field do not necessarily hold for all flows. For geometries in which the liquid must flow around obstacles, the likelihood of trapping bubbles is relatively insensitive to the wetting properties, and commercial codes with more simplified approximations to the physics also are shown to be able to give valuable information about the location of potential bubbles.

In the next section we first describe briefly the computational models and the numerical methods. The third section reports the results of the sensitivity studies undertaken as preliminary work to the code validation studies. In the fourth section we detail the experiments designed to obtain wetting parameters and material properties. Next, we report results obtained with GOMA/ARIA for the four types of geometries studied, comparing calculations with the visual observations. Then in the following two sections we review the simulations with ProCAST and MOLDFLOW. We conclude with a summary of the lessons learned and recommendations about the use of modeling in improving the encapsulation processes.

2. Numerical Methods and Computational Models

2.1 GOMA/ARIA

In order to model the most common encapsulation and potting processes, we need to model a fluid displacing air as it flows into some type of mold; therefore, we need to be able to understand both the fluid flow and its interaction with the free surface. To this end, code developers at Sandia National Laboratories have coupled the equation of motion with a level set method to determine the location of the evolving free surface [Notz et al. 2006, Schunk et al. 2002, Baer et al. 2003].

The equations of motion for the flow of incompressible, viscous fluids include conservation of momentum

$$\rho \frac{Du}{Dt} = \nabla \bullet (\mu(\nabla u + \nabla u^t) - \nabla p + \rho g + f \tag{3}$$

and conservation of mass for incompressible fluids with constant density

$$\nabla \bullet u = 0 \quad . \tag{4}$$

Here u is the fluid velocity, p is the pressure, t is time, g is the gravitational acceleration, and f includes all other body force terms. The material properties, density, ρ, and viscosity, μ, seen in Equation (3) end up as functions of both the material and the level set equation. Although in this report we will only be modeling liquids with constant μ, it is important to remember that the GOMA/ARIA codes have a sophisticated suite of viscosity models available including generalized Newtonian, viscoelastic, time-dependent curing, and suspension constitutive equations. In addition, although we will only examine isothermal flows in this report, GOMA/ARIA also solves the energy equations, and can handle the effects of heats of reactions and temperature-dependent viscosities.

The level set method of Sethian [1999], a front capturing scheme, is used to determine the evolution of the interface with time. The level set is a scalar distance function, the zero of which coincides with the free surface or fluid-gas interface, *e.g.*

$$\phi(x, y, z) = 0 \, . \tag{5}$$

We initialize this function to have a zero value at the fluid-gas interface, with negative distances residing in the fluid phase and positive distances in the gas phase. An advection equation is then used to determine the location of the interface over time.

$$\frac{D\phi}{Dt} = 0 \tag{6}$$

Derivatives of the level set function can give us surface normals, n, and curvature, H, at the interface useful for applying boundary conditions.

$$\begin{aligned} n &= \nabla \phi \\ H &= \nabla \bullet \nabla \phi \end{aligned} \tag{7}$$

Material properties vary across the phase interface from the properties of the fluid to the properties of the displaced gas. This variation is handled using a smooth Heaviside function that modulates material properties to account for the change in phase.

$$\rho(\phi) = \rho_{fluid} + (\rho_{gas} - \rho_{fluid}) H_\alpha(\phi), \qquad -\alpha < \phi < \alpha \tag{8}$$

$$\mu(\phi) = \mu_{fluid} + (\mu_{gas} - \mu_{fluid}) H_\alpha(\phi), \qquad -\alpha < \phi < \alpha \tag{9}$$

$$H_\alpha(\phi) = \frac{1}{2}(1 + \frac{\phi}{\alpha} + \frac{1}{\pi}\sin(\frac{\pi\phi}{\alpha})) \tag{10}$$

This is a diffuse interface implementation of the level set method, which allows for a mushy interfacial zone of length 2α, in which the properties will vary from fluid to gas values. Note that this method can be applied to both Newtonian and non-Newtonian fluids.

Surface tension is applied using a continuous surface stress formulation using a smooth Dirac delta function that applies this force only at the interface [Jacqmin, 1995].

$$\mathrm{T} = \sigma \delta_\alpha(\phi)\left(\underline{I} - nn\right) \tag{11}$$

$$\delta_\alpha(\phi) = \left(1 + \cos\left(\frac{\pi\phi}{\alpha}\right)\right) / 2\alpha \tag{12}$$

When using an advection equation to evolve the level set equation over time, difficulties arise as to preserving the distance function away from the interface. This is because Equation (6) only truly holds at the interface itself and using an advection equation will not preserve the distance function away from the interface. For this reason, a Huygens' algorithm is used to periodically redistance the level set function to maintain it as a distance function [Sethian, 1999].

We use versions of the Blake wetting condition (Blake and Haynes, 1969) for the wall velocity in the region of the contact line.

$$v_{wall} = v_o \sinh(b(\cos\theta^{eq} - \cos\theta)) - \tau \frac{\partial v_{wall}}{\partial t} \tag{13}$$

The value of the tangential wall velocity ramps from zero at a level set length scale away from the contact line to v_{wall} from Equation (13) at the contact line. Away from the contact line we revert to no slip for the tangential wall velocity boundary condition. The normal velocity is enforced as no penetration everywhere. The shape of this ramp must be smooth in order to get a realistic wetting line that shows a smooth transition from the contact line to the bulk flow. For a sharp transition from slip to Blake, we ended up with unphysical looking cusps in the interface shape near the wall. The transient terms allow smooth movement of the contact line.

Three versions of the Blake conditions have been used in these studies. Typically, the solid wetting surfaces have boundary conditions as follows. We apply no penetration in the normal direction

$$n_w \cdot v = 0 \tag{14}$$

and use a Navier slip condition for the tangential velocity.

$$\tau_{slip} = \frac{1}{\beta(\phi)} v_{fluid} \tag{15}$$

Here β, the Navier slip coefficient, varies from a large value near the contact line to a small value away from the contact line to enforce no slip away from the interface. A linearized Blake model enforces the dynamic contact angle condition in the interfacial region by applying a force proportional to the difference between the static and dynamic contact angles.

$$\begin{aligned} \tau_{wetting} &= v_0 \gamma\left(\cos(\theta) - \cos\left(\theta^{eq}\right)\right)\delta_\alpha(\phi) \\ n \cdot n_w &= \cos\left(\theta^{eq}\right) \end{aligned} \tag{16}$$

Here θ is the dynamic contact angle, θ^{eq} is the static contact angle, and $v_0\,\gamma$ is the wetting speed. Thus the bigger the deviation of the angle θ determined from the level set function and the set θ^{eq}, the bigger the induced stress. The stress will induce a fluid velocity at the boundary, which will move the contact line at a velocity consistent with the rest of the flow. The nonlinear version of this set of boundary conditions is identical, but equation16 is replaced by

$$\begin{aligned} \tau_{wetting} &= v_0 \sinh\left(\gamma\left(\cos(\theta) - \cos\left(\theta^{eq}\right)\right)\right)\delta_\alpha(\phi) \\ n \cdot n_w &= \cos\left(\theta^{eq}\right) \end{aligned} \tag{17}$$

Note that equation 17 results in a rate of change of the wetting velocity with the contact angle to decrease as the wetting angle deviates more and more from its static value, more consistent with physical behaviors as will be shown in Section 4.

Alternatively, in ARIA and some GOMA runs we also use a wetting boundary condition that adds the same Blake relationship between contact angle and wetting speed (equation 13), but as a Dirichlet condition on the velocity directly. This boundary condition enforces no penetration in the normal direction and the Blake velocity on the tangential direction.

The equations of motion (3-4), and the advection equation for the level set, Equation (6) are solved with the finite element method. 2D simulations were done with GOMA [Schunk et al., 2002] using a fully-coupled, Newton-Raphson numerical method and an LBB element of biquadratic velocity and level set, and bilinear pressure. The discretized equations were solved with a direct Gaussian elimination method.

3D simulations were done with ARIA [Notz et al., 2006] using a coupled velocity-pressure solve, and a decoupled level set equation. The Navier-Stokes equations were stabilized with the Dohrman-Bochev pressure stabilized pressure-projection (PSPP) [Dohrmann and Bochev, 2004] to allow for equal order, bilinear, interpolation of all variables. This stabilization method greatly improved the condition number of the discretized matrix equations, allowing for the use of an ILU preconditioner with a BiCGStab Krylov iterative solver. This was much more efficient than the previous stabilization method used, pressure stabilized Petrov-Galerkin (PSPG) [Droux and Hughes, 2000], which would allow equal order interpolation, but required a costly ILUT preconditioner with up to three levels of fill and a more expensive GMRES iterative solver. Because of the improvements of stabilization, using PSPP/ILU/BiCGStab, we ended up with computation times on the order of days instead of months for the previous method, PSPG/ILUT(3)/GMRES. Scalability was also greatly improved, allowing simulations to be run in parallel on 64 processors, giving turn around times of hours. This enabled transient design calculations on several meshes to be completed in a day.

The level set allows two materials as shown in equations 8 and 9. The density of air at 398K is 0.0011g/cm^3 and the viscosity is 2.17x10^{-4} Poise. However, to help the numerical stability, we typically use a density of the displaced air phase of 0.001 g/cm^3 and a viscosity of 0.001 Poise, which is roughly ten times higher that the actual value. Sensitivity studies (see Section 3) have shown that this makes very little difference when using the high viscosity liquids typical of encapsulation and potting processes.

Both the GOMA LBB simulations and the ARIA stabilized simulation showed good mass conservation when the constant inflow velocity results for mass as a function of time are compared to the analytical solution.

2.2 ProCAST

ProCAST is a commercial code licensed by the ESI Group, an international company that develops simulation software for various manufacturing processes – forging, casting and welding of metals, crash simulations, etc.

ProCAST is a simulation tool that uses the finite element method to model fluid flow and/or solidification in a liquid-filled cavity. The code, and its complementary simulation modules, offers the user the ability to predict heat transfer, (conduction, convection and radiation with view factors), fluid flow (including the transient mold filling process), and thermo-mechanical residual stress development. ProCAST was originally developed to simulate the metal casting process. Currently, it enjoys widespread application with foundries worldwide seeking to improve casting yields with a better understanding of the casting and subsequent solidification processes.

Most liquid-metal flows are characterized by a high Reynolds number. Casting flows are usually rapid events featuring high-density liquids (typically 7-10 g/cm^3) with low viscosities (typically 2-6 centipoise). For the current application, in which we seek to model the filling of an empty cavity with a viscous resin, the Reynolds number of the flow will be low (owing in large part to the high viscosity of the epoxy resin). Simulating flows in the low-Reynolds number parameter space is different than high-Reynolds number flows in that the character of the underlying matrix equations is different. Low Reynolds number flows impart a nearly elliptic character to the discretized flow equations. ProCAST can accommodate such flows with parameter settings, defined by the user, designed to improve algorithm efficiency in the simulation of highly viscous flow problems.

ProCAST uses a volume-of-fluid (VOF) algorithm to track the advancing fluid front through a previously tessellated region that defines the empty cavity. The fluid front is advanced within each element by solving the fluid momentum equations and, then, adjusted to satisfy mass conservation. A proprietary algorithm computes the local curvature of the advancing front by assessing the degree of fill for neighboring elements. From this information, an adjustment to the pressure field along the free surface can be computed which accounts for the effects of surface tension.

2.3 MOLDFLOW

One of the commercial tools available to review volume fills is the MOLDFLOW software program. MOLDFLOW originated from the plastics industry, moving from a strictly 2D thermoplastic injecting simulation tool of the 1980’s to a comprehensive suite of codes design for many plastic filling applications. Of merit for this project is MOLDFLOWs' capabilities to evaluate fills in 3D volumes, deriving solutions based on the Navier-Stokes set of equations. Specifically, the approach is to use a commercial tool like MOLDFLOW for first-strike filling evaluations.

MOLDFLOW is designed for filling of thermosets and thermoplastic materials where most flow is driven by a volumetric approach. Most solutions are done under uniform flow rates (as if a machine screw driving bulk material is involved). The tool does have the capability to process in a non-uniform volumetric flow manner, driven by internal pressure to overcome both wall shearing and body forces due to gravity effects. Some of the issues and limitations that the commercial tool has for the injection of encapsulants are noted below.

- High surface tension dominated flow
- Time dependent viscosity effects
- Effect of gas traps (pressure resistance)

3. Sensitivity Studies

Before beginning to compare the simulations to laboratory experiments, we first looked at how wetting, material properties, flow rate, geometry, etc. affected the likelihood of trapping bubbles in two geometries that represent salient features of Pantex and Kansas City potting processes.

3.1 Geometry 1: Pantex Notch

We are interested in the flow in narrow slots, which are common in Pantex potting processes. Geometry 1 represents flow between two parallel plates, one of which contains a notch. Earlier results using both an Arbitrary-Lagrangian-Eulerian (ALE) method and a level-set algorithm (Sun et al. 2005) showed that at small *Ca* number (0.01) a notch with similar dimensions to our Geometry 1 (Figure 1) would fill, but for larger *Ca* number (0.062) the front could skip over the notch trapping air inside. Because of the properties of the encapsulation and potting liquids, we are usually operating in this sensitive zone where completely wetting such a notch may or may not occur with only a small adjustment in parameters. To study this sensitivity in more detail we performed a series of calculations using the level-set method in GOMA.

In Geometry 1, we varied H_f/H, the inlet velocity U_{in}, and θ^{eq} of the two materials, while recording the percentage of the notch area that filled with liquid. We held the viscosity and the surface tension of the material constant, so the *Ca* was affected only by the flow rate. The expected Reynolds number ($Re=1/2H\rho U/\mu$) of a typical Pantex process is very small (O(1e-6)), and we chose a relatively high viscosity (43 Poise) to keep Re small. Table 1 shows the parameters of the base case and those of subsequent cases studied. The parameter varied in each case is highlighted in red type.

Both a linear wetting model (equation 16) and a Blake model (equation 17) were used, where v_0 was set to 10 cm/s and γ to 0.01 for the base case. Figure 2 shows that with a small γ, the relationships between the wetting line velocity $v_{wetting}$ and the dynamic contact angle are virtually identical for the two models. Examples of fits to data described in the next section are also included in Figure 2 for reference. Here, γ is over 100 times larger (O(1)) and the dynamic contact angle predicted by the linear model does not match those predicted by the Blake model as well at higher velocities. The simple linear model was one of the models available early in this study and offered the advantage of more numerical stability. The parameters of the base case linear model were chosen before the wetting data in Section 4 were available; nevertheless, the linear model wetting angles approximate the range of wetting angles seen with our materials.

A

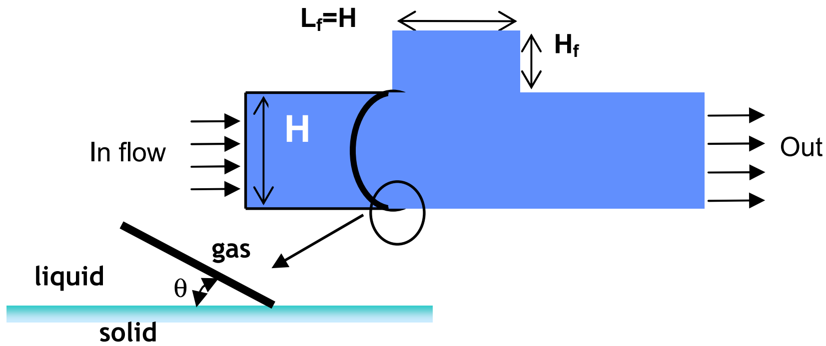

B

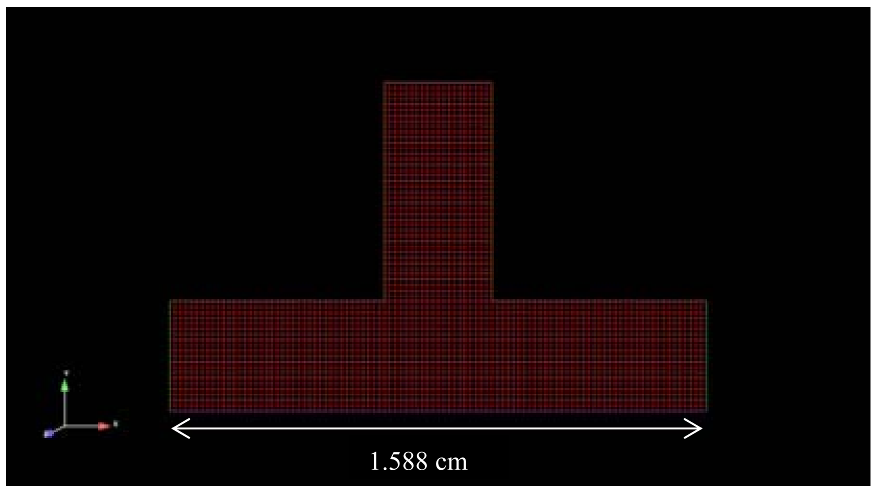

Figure 1. A. 2D representation of Geometry 1 with expanded region defining the wetting angle θ. B. Typical mesh for case in which H_f=0.635cm (1/4 inch).

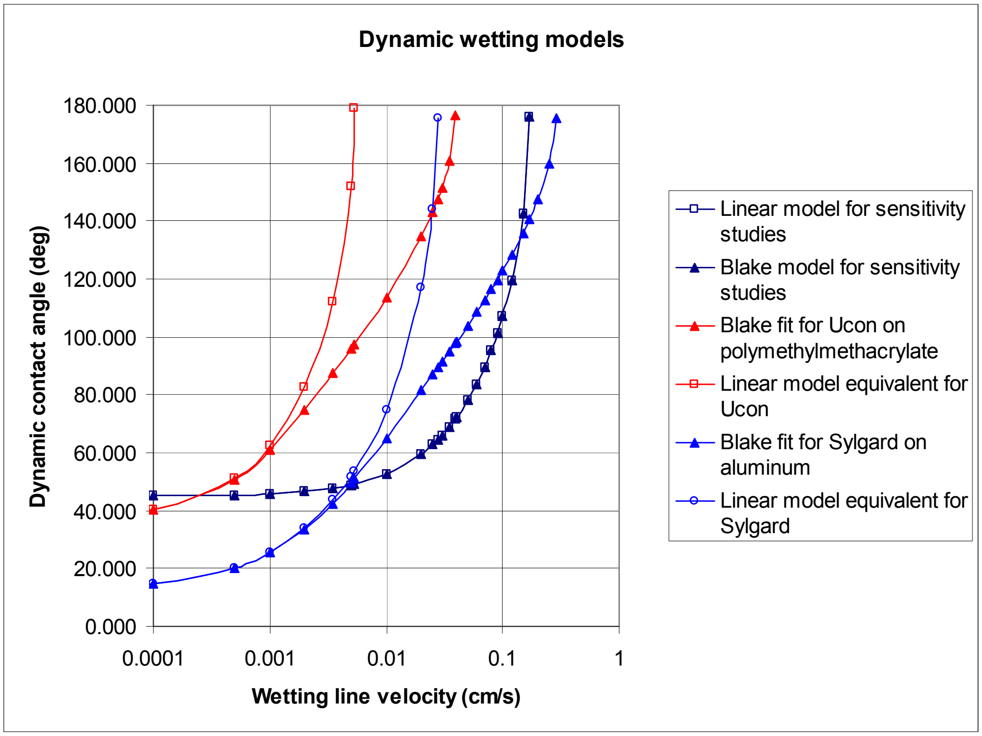

Figure 2. Relationships between the dynamic contact angle and wetting line velocity.

The results in terms of how much of the notch filled with liquid are listed in Table 1. From these results, it is apparent that if the material of the groove or notch is more wetting (lower θ^{eq}) than the material of the opposite plate, the fluid is more likely to fill the notch. Figure 3 shows results from the base case compared to those from Case 5.

These results were combined with the cases described by Sun and colleagues (2005) and were analyzed statistically with a linear effects model (Rutherford 2005) to get initial estimates of the effects of the parameters. The results are shown in Table 2 as an absolute estimated effect on the percentage of the notch area filled. In other words, as one changes the listed parameter from the lowest value to the highest value, the percentage fill is estimated to change by the amount in the last column. Negative numbers indicate that less area will fill. For example, if the notch is assumed to fill 100% with a U_{in} of 0.001, then if U_{in} is 1.0, the fill will be at most 100-83=17%. Nonlinearities were noted, and the number of cases studied was limited, so this table is included to estimate trends, not quantitative values. Nevertheless, from Table 2, it is clear that the most important effects in the range of parameters studied is the inlet velocity and the wetting of the notched material.

Table 1. Parameters varied in Geometry 1 and results

Case	**H_f/H**	**U_{in}**	**θ^{eq} notched material**	**θ^{eq} flat plate material**	**Wetting model**	**% Fill**
1 (base)	1	0.01	45	45	Linear	38.8
2	2	0.01	45	45	Linear	43.8
3	0.5	0.01	45	45	Linear	68.0
4	1	0.01	15	60	Linear	100.0
5	1	0.01	15	45	Linear	100.0
6	1	0.01	60	15	Linear	28.6
7	1	0.01	45	30	Linear	53.4
8	1	1.00	45	45	Linear	0.0
9	1	0.01	45	45	Blake	25.8

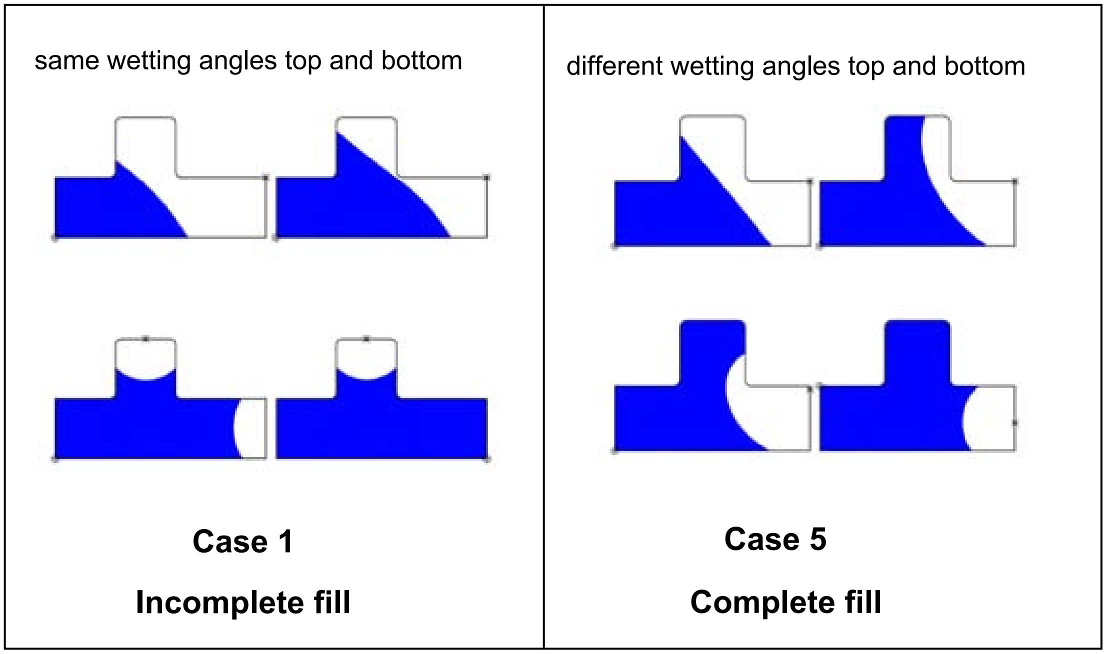

Figure 3. Results for flows with the same *Ca* = 0.01, but varying the wetting angles on the two solid surfaces. Fluid is indicated in blue as the fill progresses left to right and top to bottom for each case.

Table 2. Results of Sensitivity Study for Geometry 2.

PARAMETER	LOW	HIGH	RANGE	ESTIMATED EFFECT
H_f/H	0.5	2	1.5	-8.73
U_{in} (cm/s)	0.001	1	0.999	-83.08
θ^{eq} top.	15	60	45	-90
θ^{eq} bottom	15	60	45	-45
Linear wetting model v_0	0.1	5	4.9	-17.7
Wetting changing from linear to Blake (equivalent coefficients)				-13

3.2 Geometry 2: Kansas City Box

A more complex geometry represents encapsulation processes at the Kansas City Plant. Here a typical application involves injecting a fluid into a mold filled with electronic parts such as wires and capacitors. We represent this with our Geometry 2A, a simple 2D square mold in which four cylindrical posts are obstacles to the flow (Figure 4). This geometry was later used in the validation study, and the full 3D geometry will be discussed in the next section, as will the change in locations of the inlet and outlet.

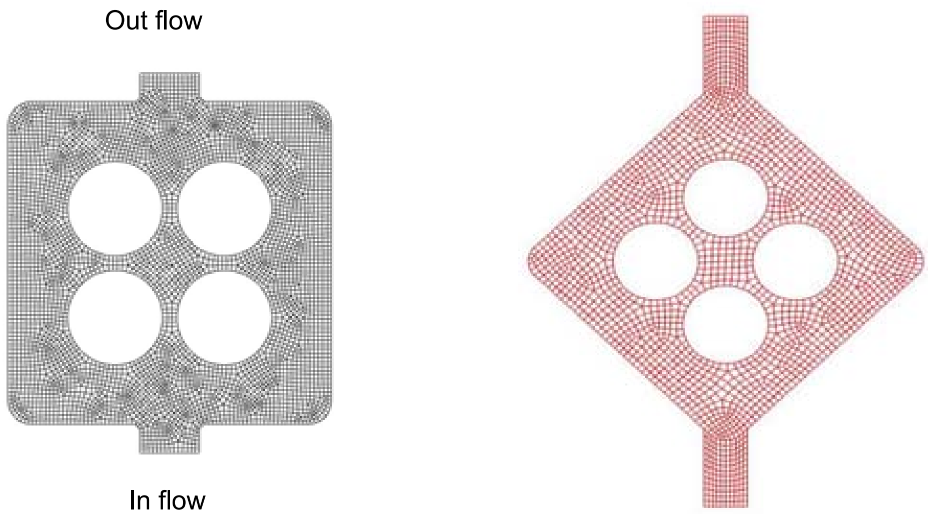

Figure 4. Typical mesh for a 2D representation of Geometries 2A and 2B.

The properties of the fluid were taken to be typical of encapsulation materials, but simplified to a noncuring liquid of high constant viscosity. Table 3 shows the parameters and results for the base case and four variations. The viscosity was varied from 300 to 2000 P, values that could be expected during use of RSF200. Again we varied the flow rate and the contact angle of the solid surfaces the fluid encounters. We assumed that all surfaces had the same wetting properties. The Blake model was used, and we looked at two wetting speeds. The Ca and Re varied with the viscosity and flow rate as shown in this table and within a range that could be expected in actual processes. The results in the table show that the volume of air trapped in the box is relatively insensitive to any of the parameters in the table, over the range of parameters we expect in the processes of interest.

Table 3. Results of Sensitivity Study for Geometry 2a.

Case	Viscosity μ (Poise)	Flow Rate q (cm^2/s)	Contact Angle θ^{eq}(degrees)	Wetting Speed v_o (cm/s)	Capillary Number	Reynold's Number	% Fill
Base Case	300	0.423	45	1	33.3	7.0e-4	87.3%
Large μ	2000	0.423	45	1	222.0	1.1e-4	89.0%
Large v_o	300	0.423	45	10	33.3	7.0e-4	88.3%
Small θc	300	0.423	15	1	33.3	7.0e-4	90.9%
Large q	300	42.3	45	1	3333.3	0.7	90.2%

The bubbles are trapped primarily because in this geometry the liquid follows the path of least resistance, creating knit lines and trapping air in the tight spaces between the obstacles. This is illustrated in Figures 5 and 6, which show numerical predictions as representative snapshots in time for the Base Case and the Large q Case. Here the trapped bubbles deform more drastically than we expect in the real material because the surface tension was chosen to be unrealistically small (12 dyne/cm) to help the numerical stability. The bubbles are convected with the fluid and some air escapes out the exit; however, even after a volume of fluid five times the volume of the box has been injected into the box, bubbles remain as seen in Figure 6.

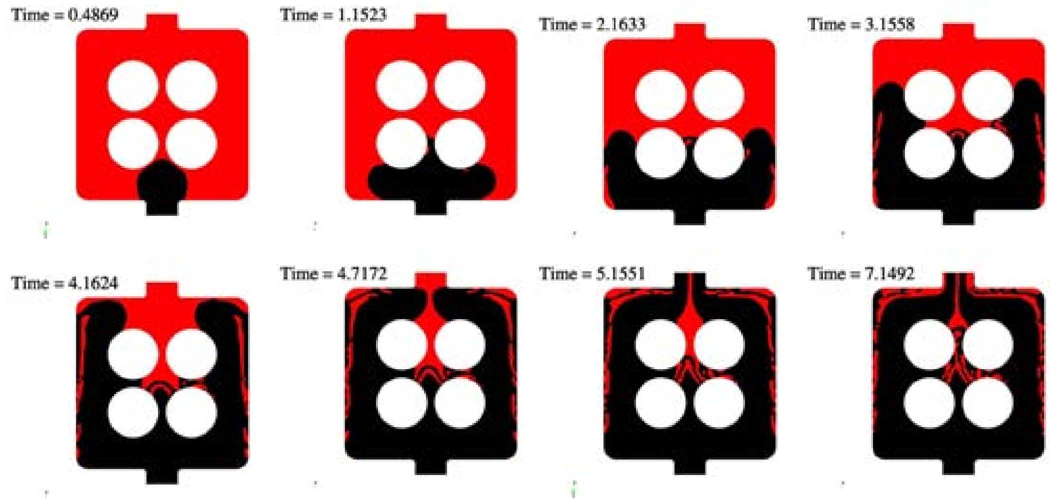

Figure 5. Time sequence from the results of the Base Case as listed in Table 3.

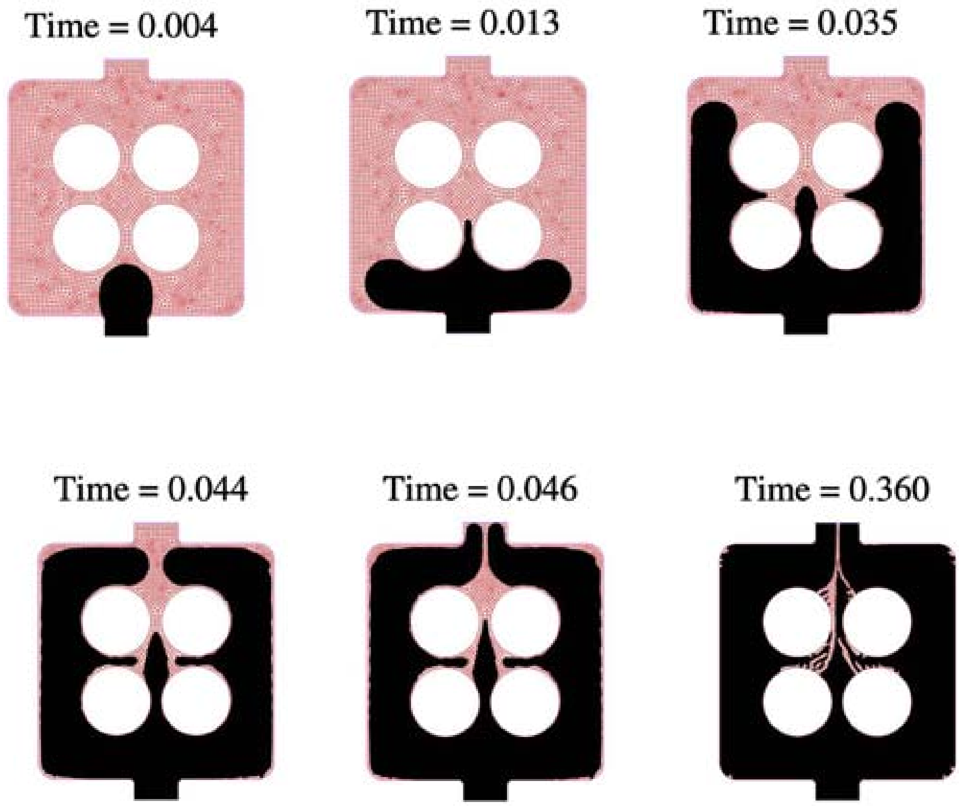

Figure 6. Time sequence from the results of the Large q Case listed in Table 3. Liquid starts to exit the top at about time=0.05s, yet at time=0.36s, when approximately 5 times the volume of the cavity has been injected, the cavity is still only about 90% full.

4. Experiments for Property Determinations

It was decided to visually record the flow liquids through transparent molds to validate the front tracking and wetting models used in the computations. Details of the geometries and experimental conditions and designation of the materials used in each test will be given in the following sections.

The liquids used were either one of a family of UCON™ lubricants (oxyethylene/oxypropylenes from Dow) or Sylgard™ 184 (a polydimethylsiloxane from Dow). The Sylgard 184 (without any added accelerant above the factory mix) is a curing material; however, rheological tests showed that the change in viscosity was negligible over the timescale of the experiments at the operating temperature of 25°C, so we chose to model this material with a fixed viscosity of 31 Pa s (Figure 7).

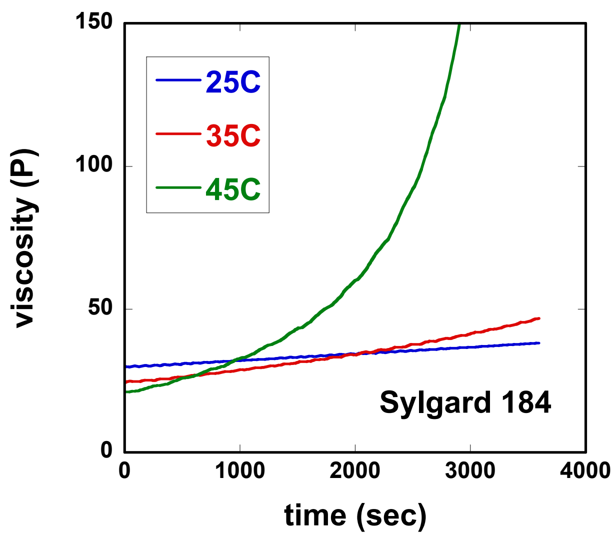

Figure 7. Rheological measurements of Sylgard 184 as functions of time and temperature. The viscosity increases only slightly over the few minutes duration of the experiments at 25°C.

The UCON lubricants were chosen because, in addition to having high viscosities, they are readily available, nontoxic, and clean up with water. The tests using these liquids were conducted at a room temperature that ranged from 23 to 24 °C. To minimize the effect of temperature on the viscosity, the liquid was held in a water bath set to 23.5°C before being used in an experiment. The viscosity of UCON 75-H-90,000 and the UCON 75-H-9500 lubricants were determined at this temperature with a Rheologica™ constant stress rheometer and were equal to 39 Pa s and 3.9 Pa s, respectively, over a shear rate ranging from 0.1 to 10 sec^{-1}.

The surface tension of all three materials were measured with a Du Noüy ring (mean circumference of 5.935 cm). The measured values for the Sylgard, UCON 75-H-90,000 and UCON 75-H-9500 were 21.7, 42.4, and 43.1 dyne/cm, respectively. A second test of the UCON 75-H-90000 with a different operator yielded a surface tension measurement of 37 dyne/cm. Batch to batch variations, contamination and moisture absorption could be attributing to the variation in the measurement.

The dynamic contact angle of each liquid on each appropriate mold material was measured in a feed-through goniometer (Brooks et al. 2006), in which liquid can be continuously injected to achieve “high” velocities, or the sessile drop can be allowed to relax to obtain “low” velocities. Figure 8 is a schematic of the experimental apparatus.

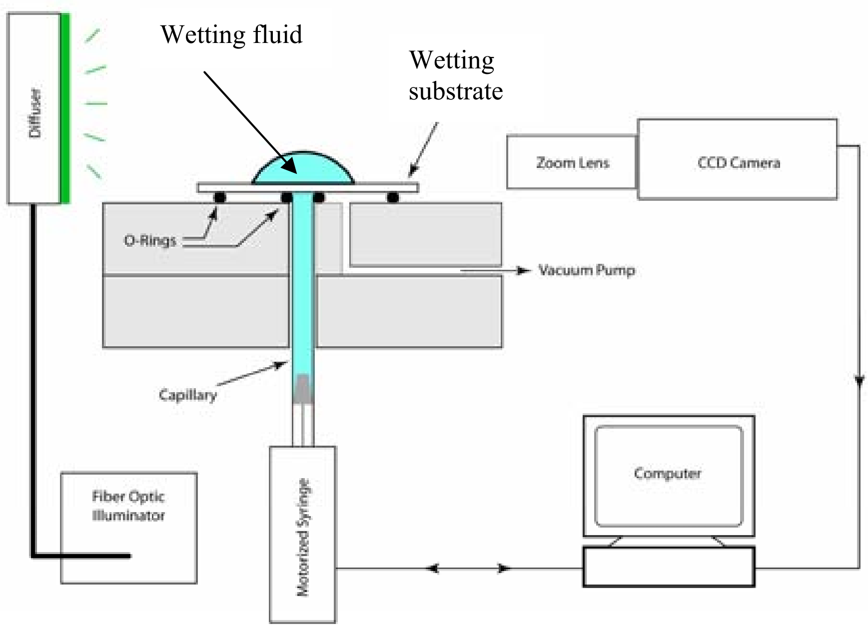

Figure 8. Sketch of apparatus for wetting parameter measurements.

During each experiment, the angle of contact and the location of the triple point of contact was recorded. The wetting line speed was then determined from the location of the triple point with time.

Figures 9 -13 show the results of these wetting tests, which were all performed at 25^{o}C. Each color represents separate tests with different injection rates and, in the case of Sylgard 184, different curing times. Results for the Sylgard 184 show that little effect from curing occurs during the time scale of our experiments at 25^{o}C. We also tested the

Sylgard elastomer base without any curative added to see the effect of the curative (in anticipation that some experiments might be done with this material so that curing would not take place at all). Although not shown in a figure, the wetting properties without the curative are reasonably different from those with and are listed in Table 4.

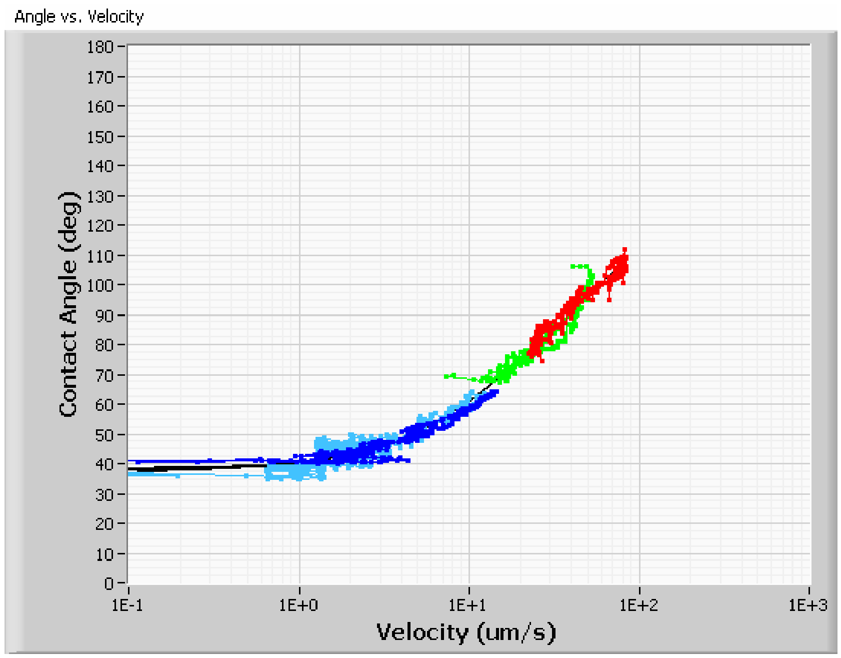

Figure 9. Dynamic wetting measurements of contact angle vs. velocity for 75-H-90000 Ucon on acrylic. Blake model fit (black line) to these data gives a wetting speed of 0.00130cm/s and scale factor γ of 2.29 with a static contact angle of 37.3°.

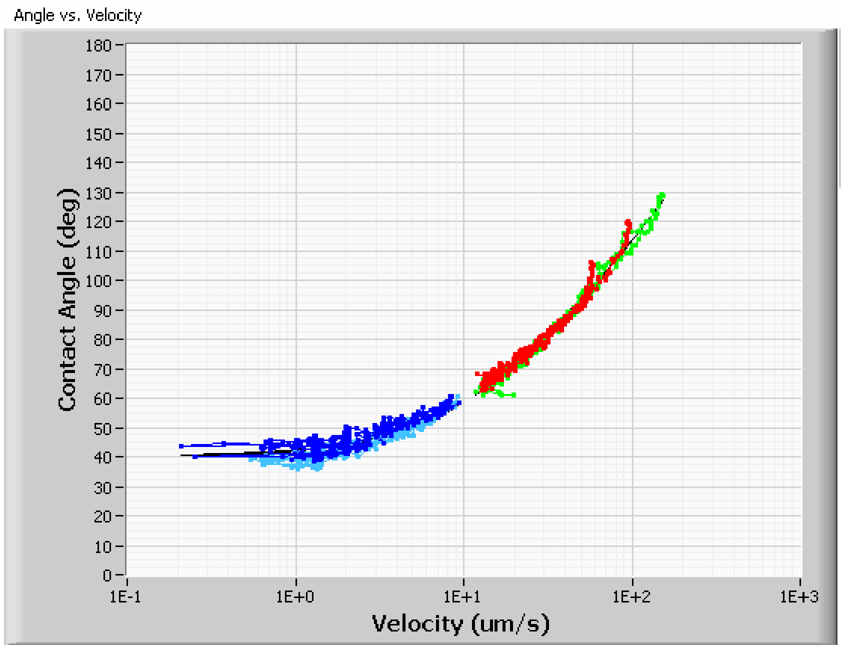

Figure 10. Dynamic wetting measurements of contact angle vs. velocity for 75-H-90000 Ucon on DSM Somos 12120. Blake model fit (black line) to these data gives a wetting speed of 0.00193cm/s and scale factor γ of 2.01 with a static contact angle of 39.8°.

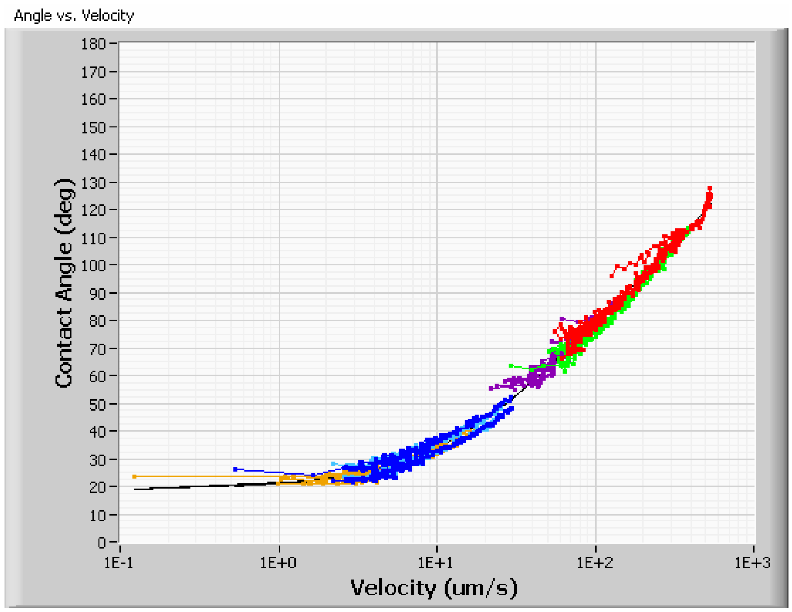

Figure 11. Dynamic wetting measurements of contact angle vs. velocity for the Sylgard 184 Elastomer base (without curative) wetting polycarbonate. Blake model fit (black line) to these data gives a wetting speed of 0.00365cm/s and scale factor γ of 2.29 with a static contact angle of 18.8^{o}.

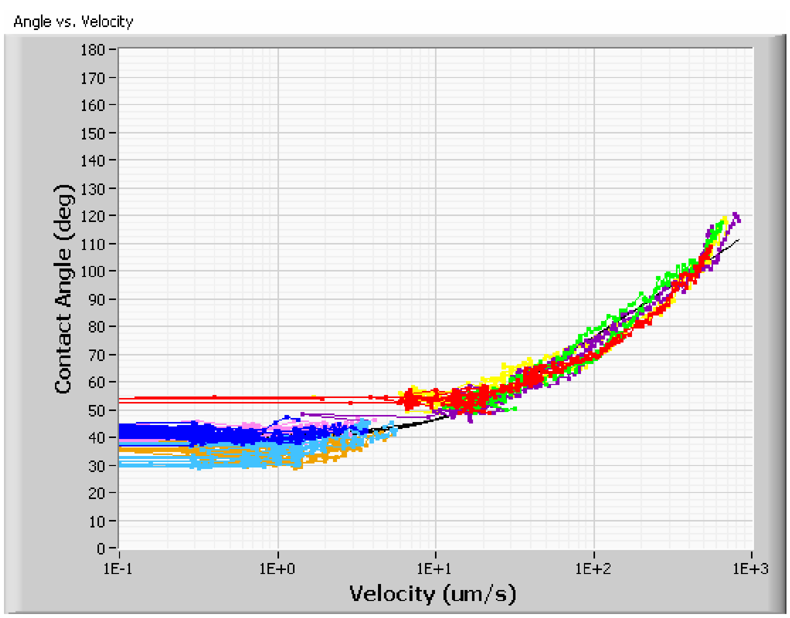

Figure 12. Dynamic wetting measurements of contact angle vs. velocity for Sylgard 184 on smooth polycarbonate. Blake model fit (black line) to these data gives a wetting speed of 0.00700cm/s and scale factor γ of 2.38 with a static contact angle of 14.8^{o}.

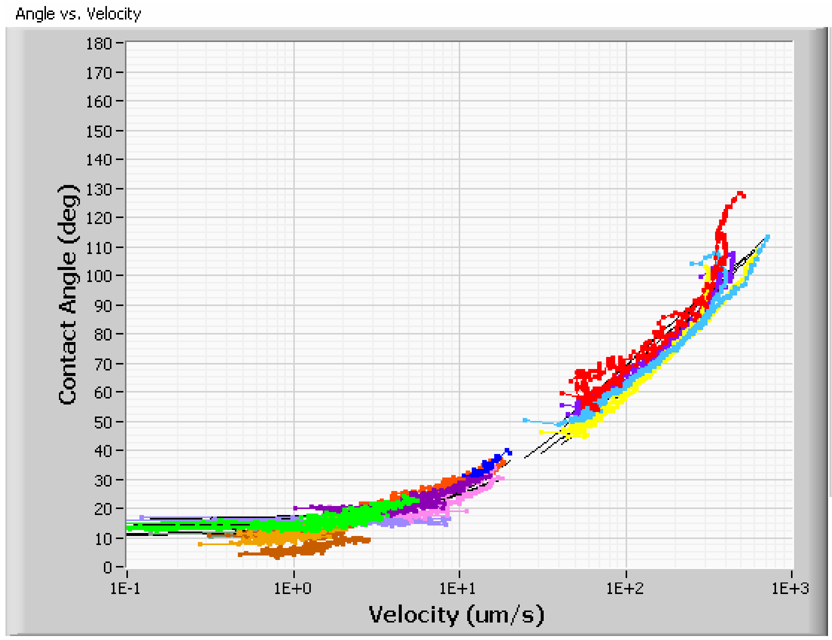

Figure 13. Dynamic wetting measurements of contact angle vs. velocity for Sylgard 184 on aluminum with a mirror finish. Blake model fit (black line) to this data gives a wetting speed of 0.00611cm/s and scale factor γ of 2.30 with a static contact angle of 13.1^{o}.

5. Validation Experiments Compared to ARIA/GOMA Simulation Results

5.1 Geometry 3: Goniometer

Our first validation study compared GOMA results in an axisymmetric approximation of the goniometer geometry to the filmed results from the wetting parameter experiments described above. Here fluid is forced through a short tube onto a plate, where it spreads both by forced convection and because of wetting and gravity forces (Figure 14). The solid surfaces are wetting surfaces and the remaining boundaries in Figure 14 are open.

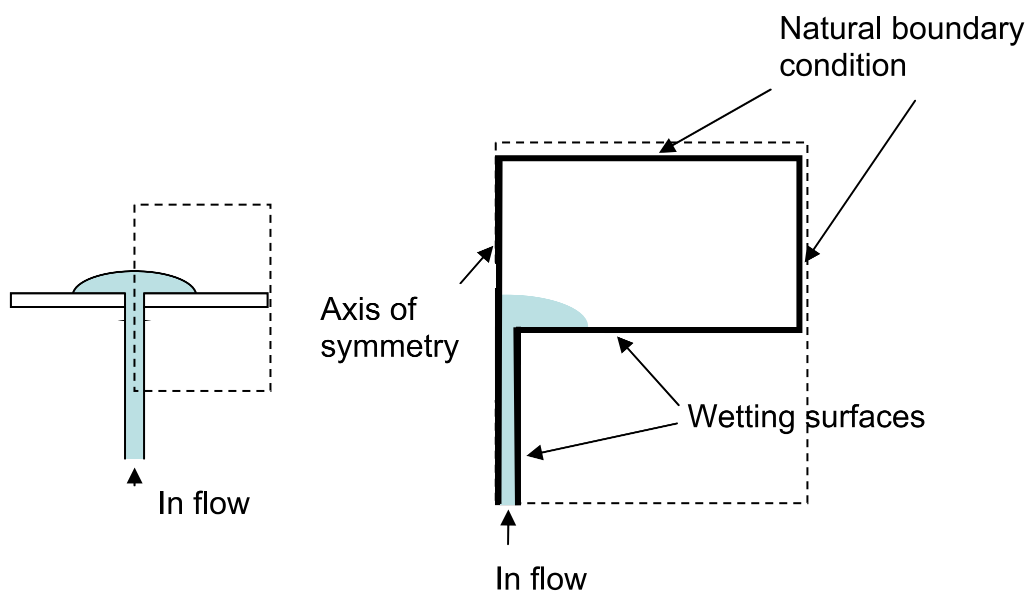

Figure 14. Simplified geometry of goniometer. Sketch, left, and 2D axisymmetric model of dotted region, right.

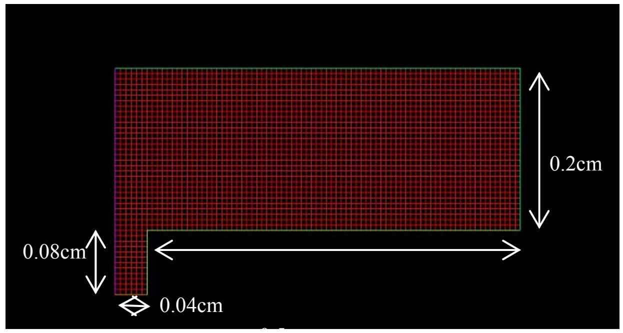

Figure 15. Axisymmetric mesh for Geometry 3.

GOMA was used on a single processor to model the flow onto the wetting substrate of the goniometer. An LBB element was used with biquadratic velocities and bilinear pressures. The extended finite element version of the bilinear pressure was used, allowing a sharp interface representation of the pressure drop across the fluid interface. This element requires no stabilization and was run with the UMFPACK direct solver.

Properties of Sylgard 184 Elastomer Resin without curing agent on polycarbonate at 25^{o}C were used in the simulation. The surface tension and gas properties were adjusted to reduce computer time. The properties are summarized in Table 4.

Table 4. Material properties used in the simulations of the goniometer.

Material Property	**Value**
Liquid density	1.03 g/cm^3
Liquid viscosity	31 Poise
Gas density	0.01 g/cm^3
Gas viscosity	0.02 Poise
Surface tension (low case)	2.17 dyne/cm
Surface tension (real)	21.7 dyne/cm
Liquid volume	0.0187 mL
Injection time (low)	7.5 s
Injection time (real)	2.5s
Blake scale factor, γ	2.29

Static contact angle	18.8^o
Blake wetting speed, v_o (real)	0.00365 cm/s
Blake wetting speed, v_o (faster)	0.0073 cm/s

In the experiment fluid was injected in the center of a horizontal plate through a 0.08cm (1/32 in) diameter hole at a constant flow rate for 2.5 seconds and then allowed to spread under the influence of gravity. In the simulation, results using this injection rate seemed unrealistic because the liquid would not wet the substrate fast enough and tended to jet upward rather than spreading.

As will be discussed in the Conclusions, we believe that the finite width of the interface (equations 8 – 10) in the numerical simulation causes the wetting to be artificially slow. We can correct for this numerical error by slowing the injection or increasing the wetting line velocity to get the correct shape of the interface as it wets. In this first case we chose to slow the injection rate. Therefore, we tried injecting the same amount of volume in the simulation as in the experiment but slowing the injection so that it took 7.5 s.

We also chose to lower the surface tension to explore the effect of surface tension on the results. Lowering the surface tension leads to better numerical stability; however, a lower surface tension increases the Bond number and influence of gravity. Consequently, the shape of the spreading drop deviates from the spherical cap that is observed at low Bond number in the experiments.

Figure 16 shows representative snapshots of the results compared to the experimental data for Sylgard 184 elastomer without curative wetting polycarbonate.

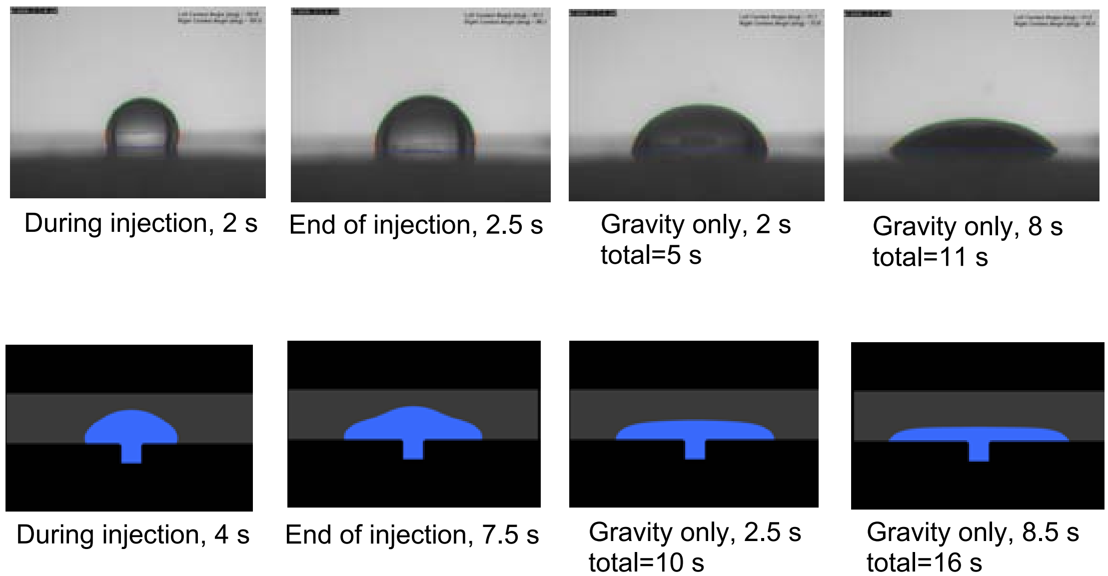

Figure 16. Experimental recording (top) and GOMA simulation (bottom) of a spreading drop of Sylgard elastomer base without curative on polycarbonate. Here the surface tension in the simulations is lowered by a factor of 10 from the actual properties and the injection rate is also lowered.

We also performed a calculation with the correct surface tension and correct injection rate, but increased the wetting speed to twice the measured speed. In this case, the droplet shape looks more realistic and the actual injection rate can be used. A movie of this process shows the fast change in size during injection and then the slow relaxation where the wetting angle decreases as the velocity of the triple point slows. From this study we concluded that if an expedient was needed to achieve numerical convergence or a more realistic behavior, it was better to increase the wetting speed artificially than to lower the surface tension and flow rate.

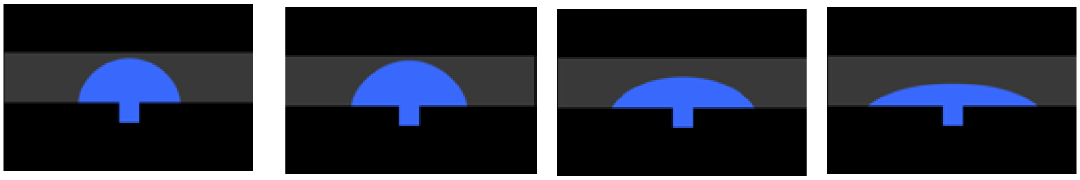

Figure 17. GOMA simulation and experimental recording of a spreading drop of Sylgard elastomer base without curative on polycarbonate. Here the wetting speed v_0 in the simulations is increased by a factor of two from the actual properties.

5.2 Geometry 1: Pantex Notch Revisited

As discussed in the section about the initial sensitivity studies, Geometry 1 represents flow between two parallel plates, one of which contains a notch. The apparatus (Figure 18) consists of a machined aluminum flat plate and a polycarbonate plate in which grooves have been machined. Each plate is about 10 cm long by 10 cm wide. These plates are held apart with a gap of 0.318 cm (1/8 inch). The fluid flows up, against gravity, through a distributor region with two wells, which was designed to create a relatively flat flow front entering the gap between the plates. The distributor's triangular shape was designed using GOMA. Figure 19 shows the front shape calculated with the originally proposed inlet geometry and with the triangular distributor.

The center-to-center distance between notches is 2.86 cm (1.125 inch), which we estimated would be large enough that the front approaching a notch would be unaffected by the previous notch. The polycarbonate material allows visibility from both top and sides.

Sylgard 184 was injected with a MIXPAC pneumatic delivery system using a 200 ml cartridge system and an inline mixer with 24 turns. A flow rate of approximately 0.5 cm^3/s was used. Photos were taken from the side (Figure 18B) and from the front (Figure 18A), although not in the same experiment. Photos from the front showed that the fluid interface was reasonably straight as it approached each notch (Figure 20).

As mentioned above, Figure 1 shows a 2D approximation to this geometry. Here the plates and groove are assumed to be infinite in the direction out of the paper. In addition to the sensitivity studies above, this geometry has been used in previous work using GOMA by Reddy et al. [2005] . Although studied before, here we validate the solutions at moderately high *Ca* with experimental data. Here, H=0.318 cm, and H_f=0.159, 0.318 or 0.635 cm.

A

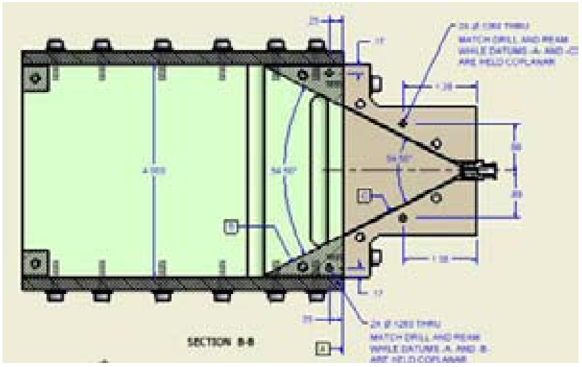

B

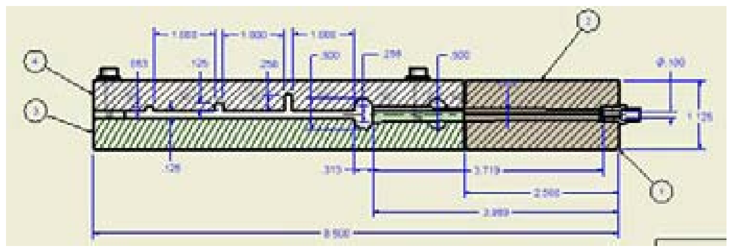

Figure 18. Two views of the apparatus used to test Geometry 2 with dimensions in inches. A. The triangular area on the right acts as a distributor. B. Region 3 is aluminum, and 4 is polycarbonate.

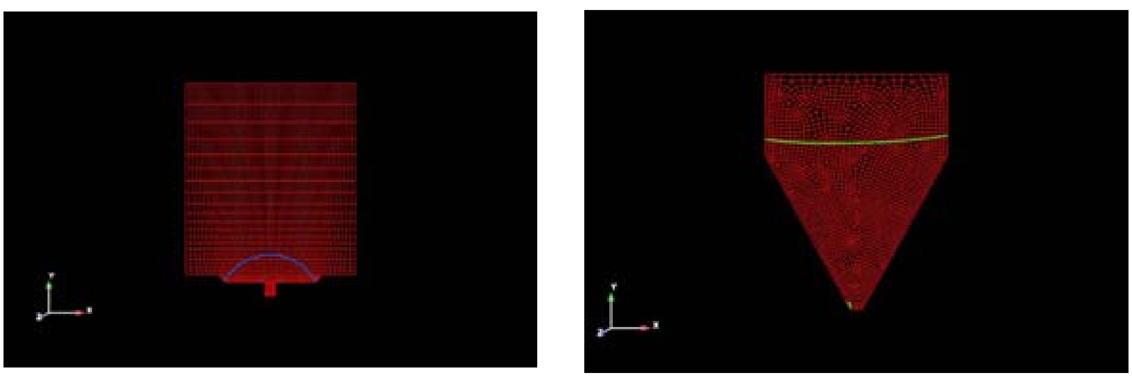

Figure 19. Flattening of flow front with a change in distributor shape predicted in a 2D GOMA calculation.

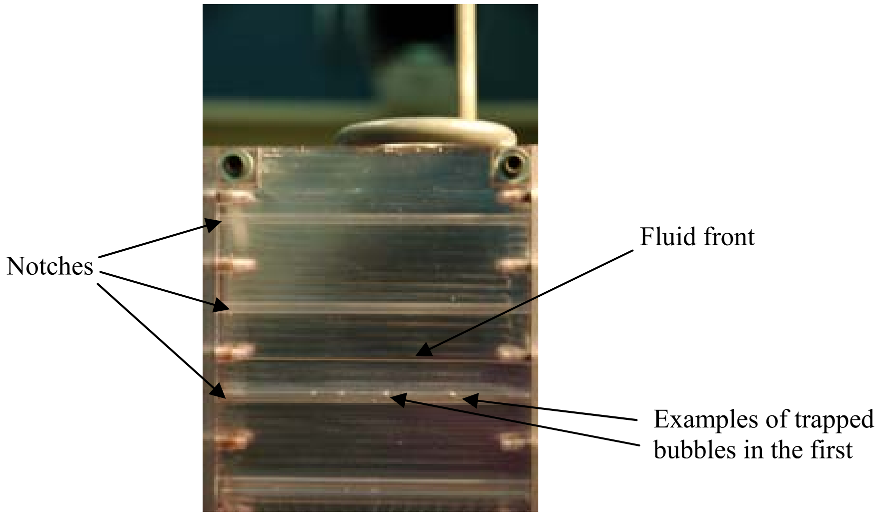

Figure 20. View of notch validation study showing relatively flat front between notches.

ARIA was used to model in 2D the flow past the three sizes of notches using the properties of Sylgard 184 without added accelerant on polycarbonate (PC) and aluminum (Al) at 25°C. To test the sensitivities of the results we also simulated the flow using properties of the Sylgard elastomer without any curative. These values are summarized in Table 5.

Table 5. Material properties used in the notch simulations

Material Property	**Value**
Liquid density	1.03 g/cm^3
Liquid viscosity	31 Poise
Gas density (low)	0.001 g/cm^3
Gas density (high)	0.01 g/ cm^3
Gas viscosity (low)	0.002 Poise
Gas viscosity (high)	0.02 Poise
Surface tension	21.7 dyne/cm
Inlet velocity	0.06 cm/s

Blake scale factor, γ PC	2.38
Blake scale factor, γ PC (no curative)	2.29
Static contact angle PC	14.8 ^{o}
Static contact angle PC (no curative)	18.8^o
Blake wetting speed, v_o PC	0.00700 cm/s
Blake wetting speed, v_o PC (no curative)	0.00365 cm/s
Blake scale factor, γ Al	2.30
Blake scale factor, γ Al (no curative)	1.81
Static contact angle Al	13.1 ^{o}
Static contact angle Al (no curative)	18.9^o
Blake wetting speed, v_o Al	0.00611 cm/s
Blake wetting speed, v_o Al (no curative)	0.00728 cm/s

Fine structured meshes with 20 elements across the channel were required to minimize mass loss in the level set calculations. Increasing the gas density and viscosity by a factor of 10 to the values labeled "high" in the table reduced computer time by a factor of 3 but had negligible effect on the results. The flows were modeled with the ARIA code and required less than 12 hr of computer time run on a single processor with the low values of gas properties. An LBB element was used with biquadratic velocities and bilinear pressures. This element requires no stabilization and was run with the UMFPACK direct solver.

Figures 21-22 show results, both experimental and numerical, for the medium and short notches, respectively. Figures 23 and 24 show the results for the long and short notches, but simulated with the properties of the elastomer without curative. Note that in 2D, when the fluid front hits the far corner of the notch air is immediately trapped. The front goes up the far side of the notch only a short distance after this occurs. In the real case the front we see in these photos is only immediately next to the transparent side wall. In the center of the flow, away from this side wall, the fluid front hits the notch at a slightly different time, allowing flow in the direction of the notch (perpendicular to the paper in the figures) and more air to escape than is possible in the 2D simulations. Therefore, we see the liquid move farther along the far side of the notch in the real case than in the 2D approximation (circled region in Figure 23). Therefore, the 2D simulation gives conservative results in the sense that the trapped bubble appears larger than it would be in real life. Although clearly one must be careful when interpreting 2D results and inferring the real world equivalents, the simplified model can predict trends such as the fact that a bubble does indeed get trapped and the relative sizes of the bubbles in the various notches.

In Figures 21 and 22 it appears that, in the experiment, bubbles may be trapped in both the top and bottom corners of the notches after the front goes past. It is not clear, however, because lighting the side of a wide apparatus like this one is difficult. Also, as can be seen in Figure 24, sometimes bubbles were injected into the apparatus or formed during flow before the notch in question and were convected along with the interface. The bubbles that appear in the bottom corner of the notch in the experiment may be of that type and be farther away from the wall initially (see the faint outline of a circle in the first images) and then show up more clearly later because of 3D flow effects.

In the 2D simulations with the real properties only one bubble is trapped. However, whether one or two are trapped is a function of how the front approaches the walls. As mentioned above, the diffuse interface in the simulations seems to cause the wetting angle to actually be higher than the model input parameters. However, if an even higher angle is used as input (properties of the elastomer without any curative), the simulation actually predicts two bubbles in the shortest notch (Figure 24). This dramatic change in results from changing input properties as seen in the short notch illustrates how sensitive filling this geometry is to wetting properties, as discussed in the sensitivity studies above. Because of the sensitivity, it is also the most difficult to model, even though the geometries in the next two sections are more complex.

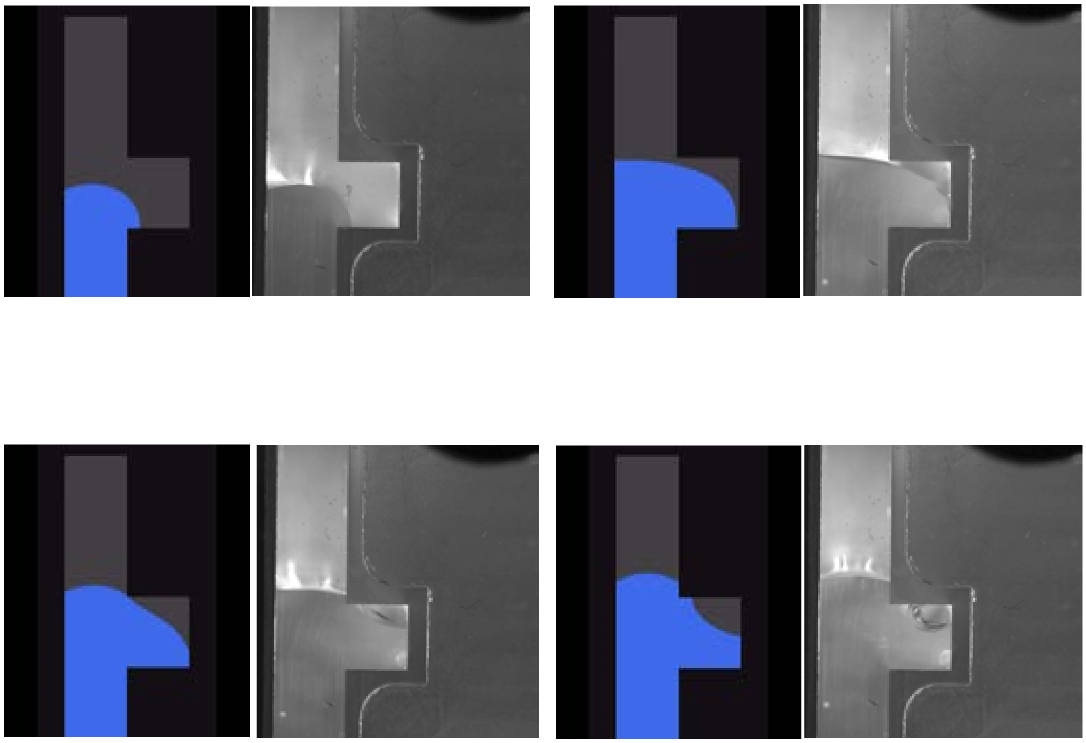

Figure 21. Representative frames from ARIA simulations (left of each pair) and visual observations (right) of the flow in Geometry 2 with H_f/H=1.

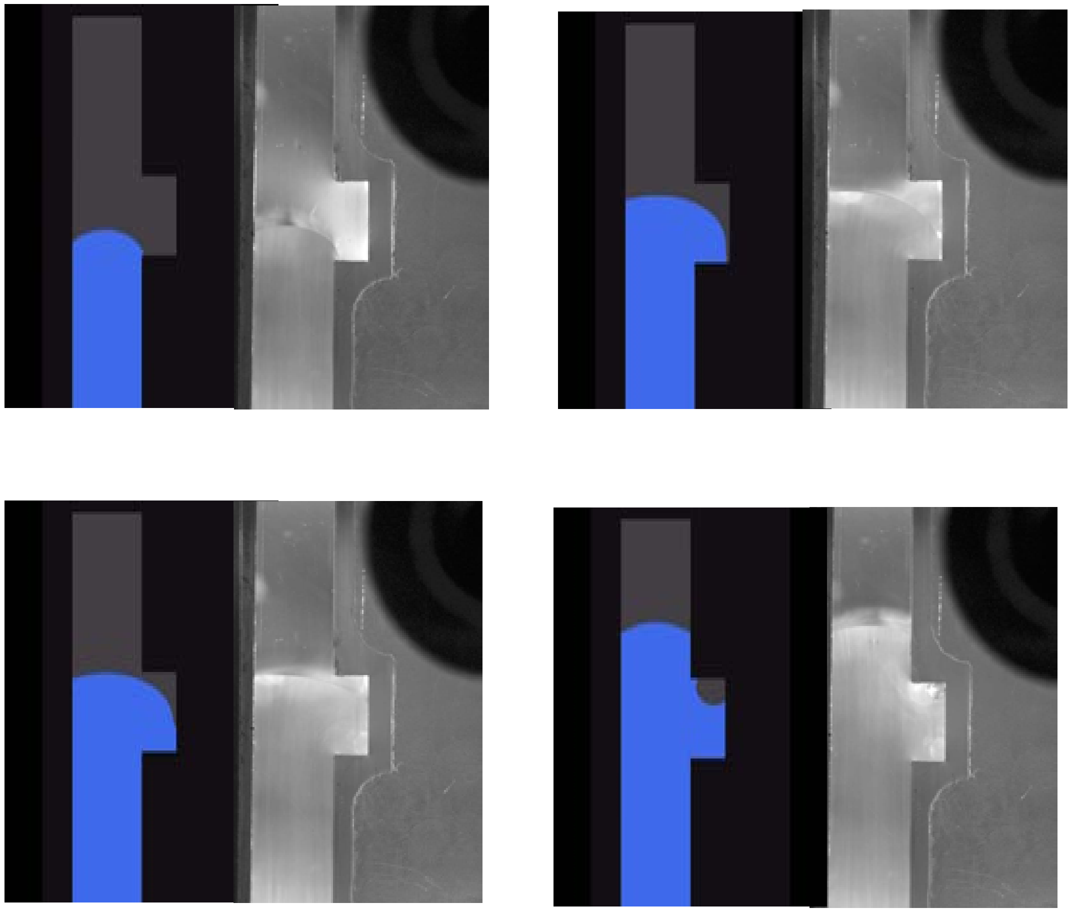

Figure 22. Representative frames from ARIA simulations (bottom) and visual observations (top) of the flow in Geometry 2 with H_f/H=0.5.

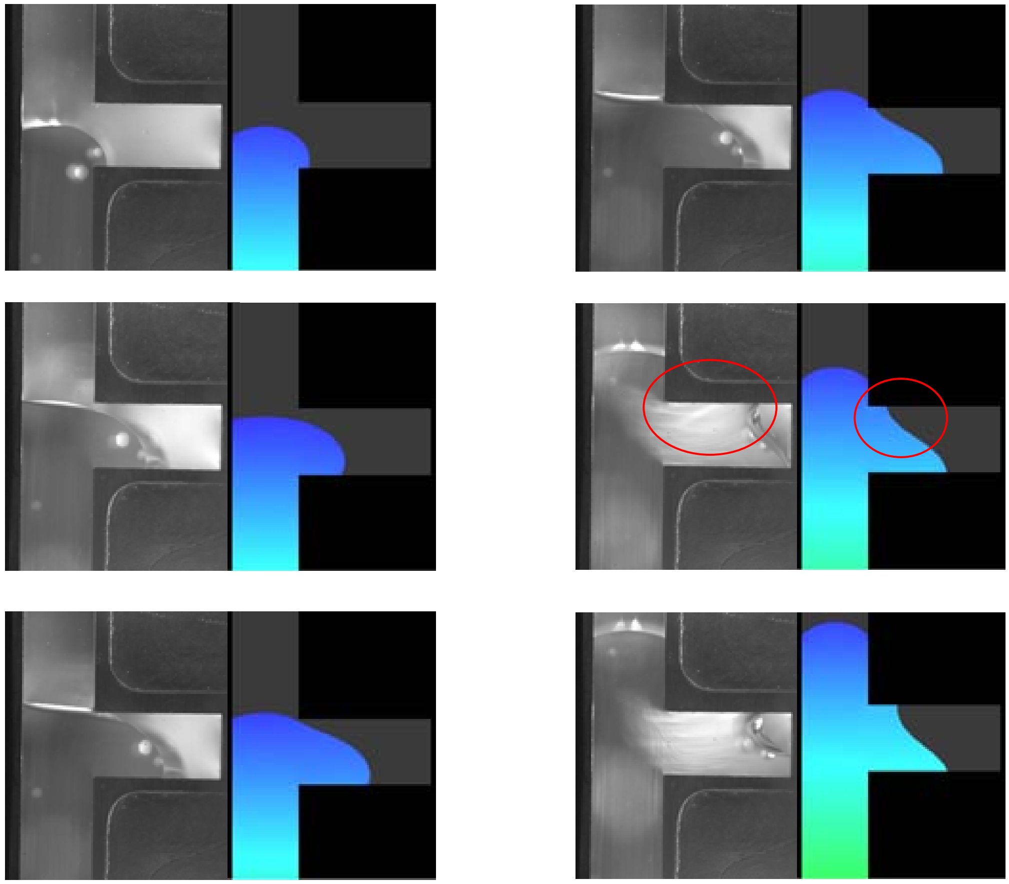

Figure 23. Representative frames from ARIA simulations (right side of each column) and visual observations (left side of each column) of the flow in Geometry 2 with $H_f/H=2$ (Figure 5). Experiment used the curing system and the simulation is for the elastomer only. Circled region indicates the difference between 3D and 2D as discussed in the text. Color gradations indicate pressure.

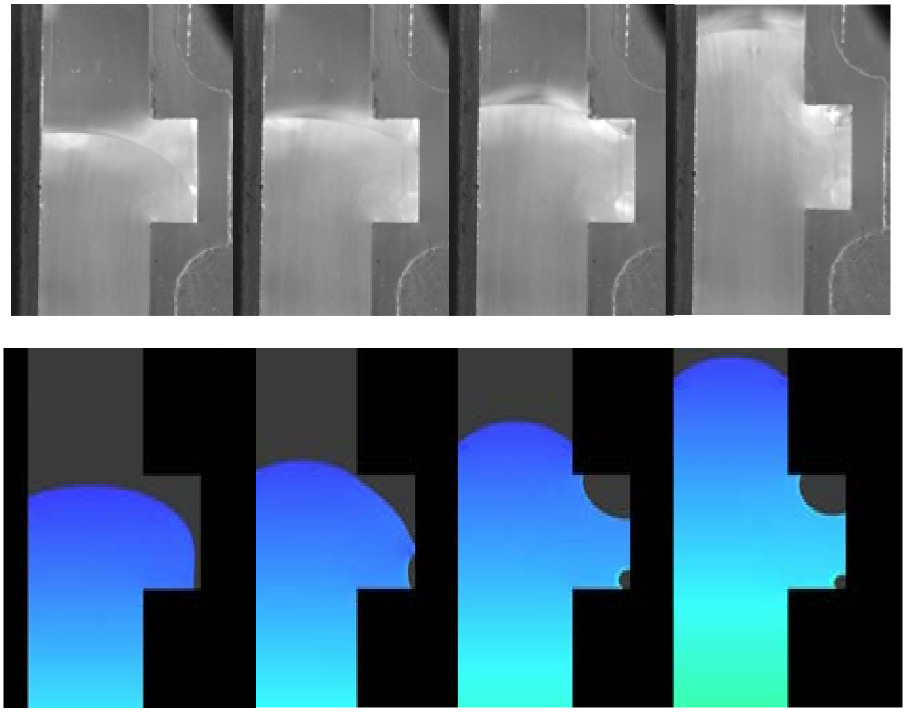

Figure 24. Representative frames from ARIA simulations (bottom) and visual observations (top) of the flow in Geometry 2 with H_f/H=0.5. Here simulations used wetting properties of the elastomer without curative, somewhat less wetting than the Sylgard 184 complete system. Color gradations indicate pressure.

We modeled Geometry 1 in 3D; however, to minimize the computational time we decreased the width of the apparatus substantially. We also simplified the calculations by assuming the same wetting properties on both plates and on both side walls – that of the elastomer without curing agent. The simulations were run using ARIA with stable hexahedral elements, specifically quadratic velocity and linear pressure elements (Q2Q1). An iterative solver involving GMRES with ILU preconditioning was used to solve the resulting linear system of equations. While this element/solver combination has been problematic for 2D quadrilaterals, good experience was obtained for these 3D, level set simulations. Typical simulations ran in less than 8 hours on 32 processors of Sandia's Thunderbird Linux Cluster.

Figure 25 shows some representative snapshots from the computations. The fluid level does travel up the notch on the wall side more than in the 2D calculations. Here the bubble still appears to span the entire width of the apparatus. Visual observations of the experiment looking into the face of the apparatus (Figure 20) show that the air trapped when the front crosses a notch tend to break into individual bubbles. Most likely this is a function of physics that are not fully captured even in these sophisticated numerical models.

Finally, we continued the flow past the notches once the bubble was trapped. The simulations never showed a bubble tending to escape from the wall to be reintroduced into the flow. However, operator testimony states that bubbles did escape the notches after the flow stopped, although this happened over night with no witness as to how this actually occurred. Detachment of bubbles from a surface includes complex phenomena that is not captured in the current models and is beyond the scope of this project to research and develop.

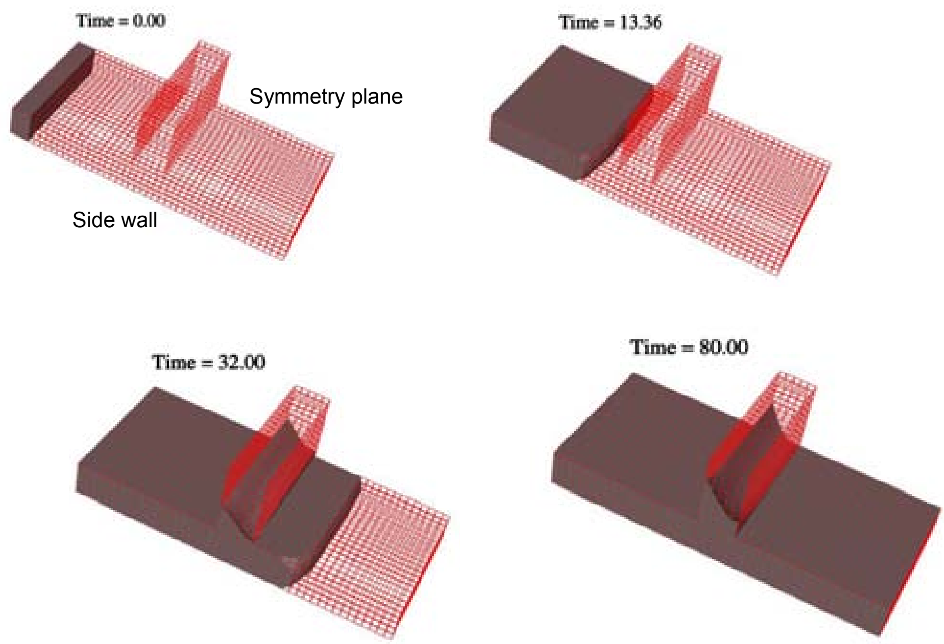

Figure 25. ARIA 3D simulation results of notch problem.

5.3 Geometry 4: Injection Molding

In addition to the single-notch geometry of Figure 25, we include a simplified 3D version of the entire parallel plate geometry (Figure 18). This geometry consists of an inlet pipe expanding through a distributor into an empty box as shown in Figure 26. Here there are no notches and, although reminiscent of Geometry 1, each are about 5 cm in the longest direction. This geometry also is similar to many manufacturing processes where a cavity must be filled with an encapsulant and wetting at the corners is important. The effects of three different distributors and two orientations are studied. These geometries were first studied both to validate the GOMA/ARIA coupling of the level set method to the wetting models and to help design a proposed injection molding process [Rao et al. 2006]. Details of the model and comparison to laboratory data can be found in the above document; however, a brief review of this work will be given in the present report for completeness, as well as results of some more recent work.

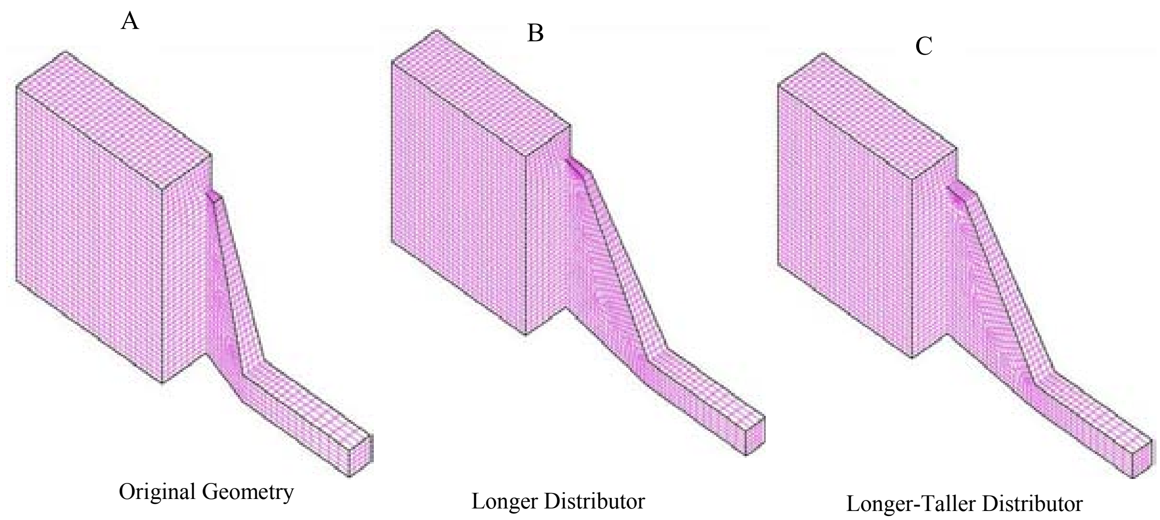

Figure 26. Geometry 4 with various distributor shapes. A plane of symmetry allows us to only mesh one-half of the geometries (see Figure 27).

Molds made to the same size specifications as the meshes were fabricated out of acrylic. A pressure driven syringe filled with UCON 95-H-90000 was held at a constant pressure during injection. The syringe of liquid was degassed in a vacuum chamber prior to the experiment. Here, the syringe was modified to prevent leakage around the plunger and subsequent bubble formation. However, this resulted in more friction and a flow rate that varied somewhat from experiment to experiment. Hence, the time to fill the molds varied from test to test, but was determined and recorded for each test. The tests were conducted at a room temperature that ranged from 23 to 24^{o}C. To minimize the effect of temperature on the viscosity, the liquid was held in a water bath set to 23.5^{o}C after degassing and before being used in an experiment.

Calculations were made with ARIA of flow in these geometries both with the flow parallel but against gravity (vertical orientation) and with the flow perpendicular to gravity (horizontal orientation). Figure 27 shows the boundary conditions.

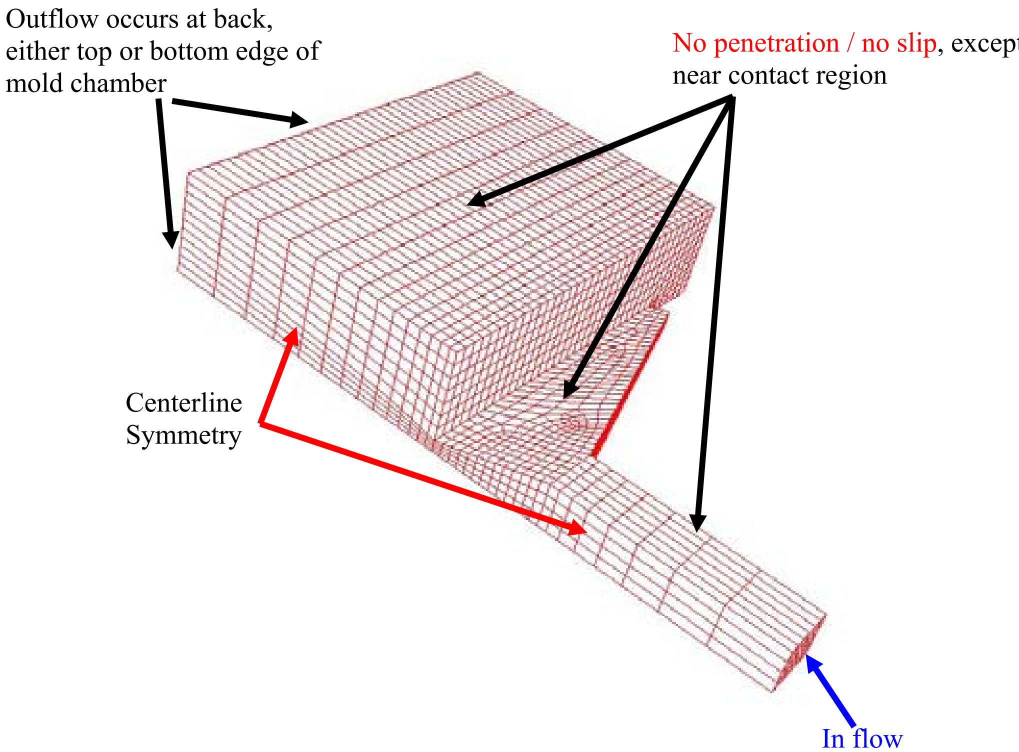

Figure 27. Typical 3D mesh and boundary conditions for Geometry 4A. The outflow vent is on the same side as the distributor for vertical simulations and opposite the distributor for horizontal simulations.

Properties used for the validation simulations were the measured values of the UCON 95-H-90000 discussed in the previous section. The density and viscosity of the displaced gas phase were taken as fictitious value of 1000 smaller than the liquid phase density and viscosity. These values are summarized in Table 6.

Table 6. Material properties used in simulations of Geometry 4.

Material Property	**Value**
Density of liquid	1.09 g/cm^3
Viscosity of liquid	390 Poise
Density of gas	0.0011 g/cm^3
Viscosity of gas	0.39 Poise

Wetting speed, v_o	0.0013 cm/s
Blake scale factor, γ	2.29
Static contact angle	37.3^o
Surface tension	42.4 dyne/cm
Inflow pressure	1e6 dyne/cm^2

At 100^{o}C, the viscosity of air is $2.17\text{x}10^{-4}$ Poise and the density of air is 0.0012 g/cm^3, thus our second phase properties are very close for density, but three orders of magnitude too high for viscosity. The numerical method fails to converge for values of the liquid/gas viscosity ratio of less than 1000 for a diffuse interface implementation of the level set equations.

For the inflow condition, we used a constant inflow pressure of 1.0 e6 dyne/cm^2. This value was chosen to roughly match the horizontal fill time of 23 seconds in the original mesh and then used for all other meshes and geometries. A shooting method was used, where different values of the inflow pressure were used and the solution was examined to see if it filled in the correct time. This required many simulations to be run. It is believed that the actual boundary condition for the experiments is somewhere between a constant velocity and constant pressure condition, but this is hard to replicate numerically. From the simulations we did find that the velocity changed quickly in the beginning for the pressure inflow boundary condition and subsequently reached a steady value.

The simulations were run using ARIA with PSPP pressure stabilization and the BiCGSTAB/ILU solver-preconditioner pair. This stabilization method has shown good scalability and robustness, allowing for a fast Krylov based solver with low levels of preconditioning, all of which means quick turn around times for solutions. The validation runs were made on 64 processors of Sandia's Thunderbird Linux Cluster and ran in less than 3.5 hours.

Figures 28 and 29 compare representative frames from the video recordings of the fill process using a vertical alignment of the mold compared to model predictions. The time it took in the laboratory experiments to completely fill the original geometry 4A (so that liquid was beginning to exit along the entire length of the vent) was 24.6 ± 1.2 s, to fill geometry 4B was 26.9 ± 2.0 s, and to fill the geometry 4C was 24.6 ± 2.3 s. Because the volumes are different, the fill rates varied between geometries. This and the fact that experimental variability exists led us to represent times in a nondimensional form.

The times to fill the mold in the calculations for the vertical orientation for 4A, 4B, and 4C were 15.2s, 17.5s, and 13.2s, which were much faster than the experimental values. We defined our fill time as when the vent had filled completely to a distant of the level set length scale or two elements. Unfortunately, the numerical fill times are difficult to obtain accurately as the gas phase viscosity makes a large difference in how fast a simulation will fill for the same value of pressure. For instance, when we reduced the second phase viscosity by a factor of 10 we got an increase in the inflow velocity when keeping all other parameters constant. So the fact that the gas phase is harder to push out than it is for the experiments, adds a great deal of uncertainty to the fill times. However, we hope to be able to predict trends.

The initial time is taken to be when the front passes a line in the square entry channel 0.16 cm from the entrance of the distributor. In 3A quite a bit of fluid enters the main cavity before completely filling the distributor. As detailed in another report (Rao et al. 2006) we modified the distributor shape to attempt to flatten the fluid front entering the main cavity. In Figure 28, one can see the effects of changing the distributor geometry.

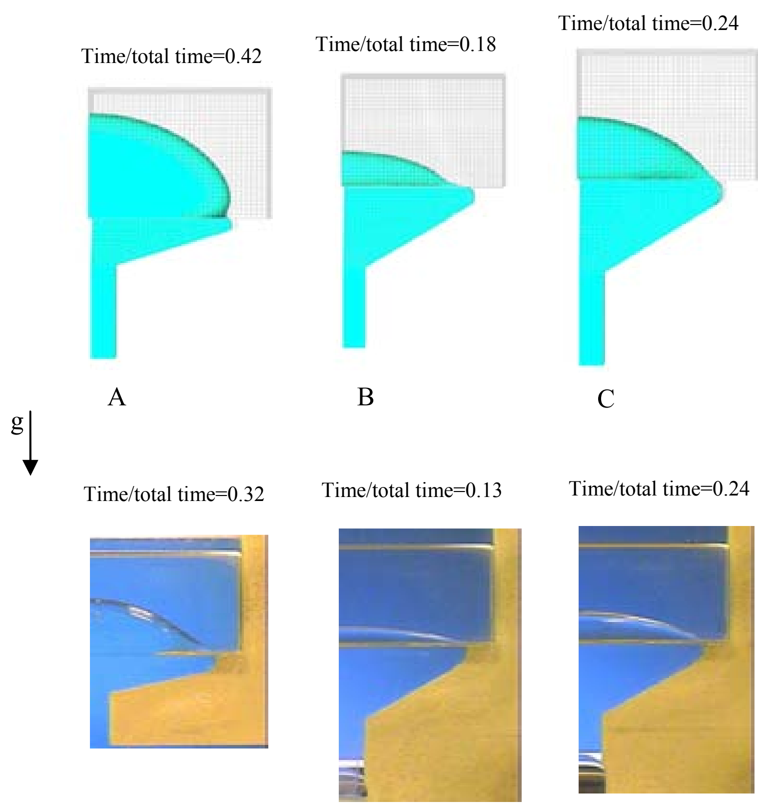

Figure 28. Comparison of the effect of distributor geometry on the shape of the fluid front entering the mold for vertical orientation of Geometry 4A-C.

As predicted by numerical results, the two modified geometries help flatten the leading front, especially 4B. The distributor in 4B also fills with the fastest relative time. Comparing the numerical and experimental version of this profile, we can see that the simulations are catching the correct trends of the physical situation. The original mesh takes the longest fractional time to fill the distributor, 42% numerically and 32% experimentally, and gives the most bulging front shape. 4B is an improvement, taking 18% numerically and 13% experimentally of the time to fill the distributor, while 4C is somewhere in between at 24%.

Although the numerical calculations do a good job of predicting the trends caused by the change in distributor design, the shape of the leading front does not match exactly. The shape of the meniscus for 4A has more of a bulge at the edge of the distributor than the experimental one, which looks as if the front is pinned at the distributor.

Better matches to the shapes could be obtained by modifying the wetting line speed from that measured in the goniometer, as was seen in Geometry 3 and will be discussed more in the conclusions.

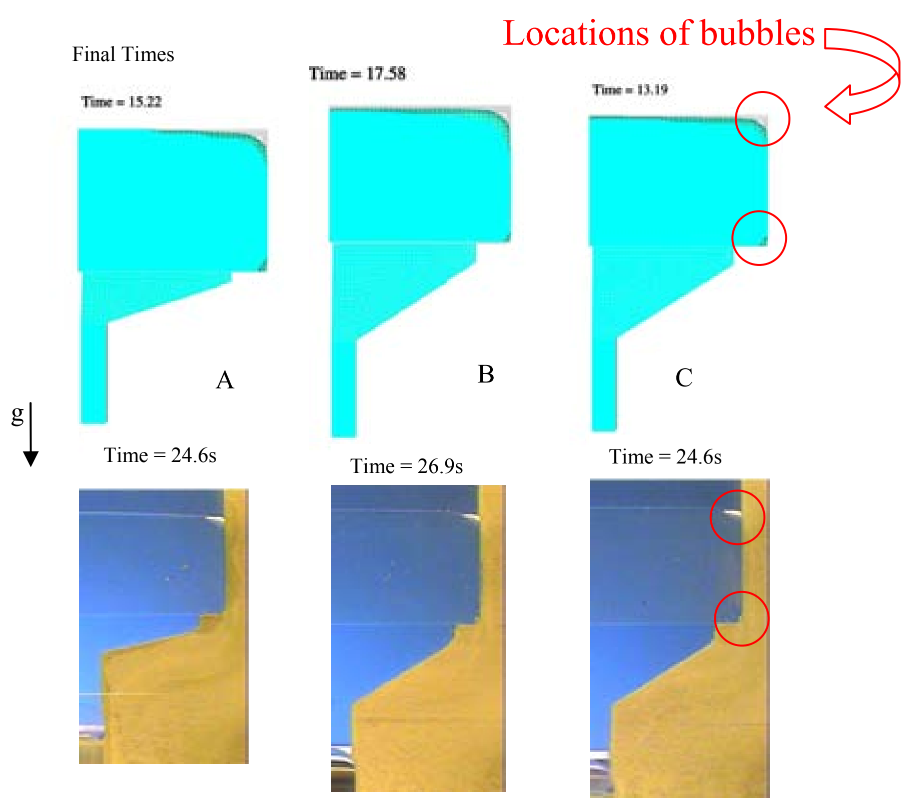

Figure 29. Comparison of the effect of distributor geometry on the location and size of final bubbles with the apparatus in a vertical orientation.

Figure 29 shows the locations of bubbles remaining as the fluid just fills the main cavity (without any overpressure). Small bubbles in the experiment away from the corners are artifacts of the syringe loading process. The voids in geometries with redesigned distributors still remain in the same locations as those seen in the original geometry. The relative areas of the bubbles on the images, which reflect the volume of air trapped, were determined. The area of the upper corners were measured to be 0.0153 ± 0.0012 cm^2 for 4A, 0.0086 ± 0.0007 cm^2 for 4B, and 0.0128 ± 0.0005 cm^2 for 4C. In the experiment, one pixel resolution represents about 1×10^{-5} cm^2. The lower bubbles near the distributor are much smaller than the upper ones. The calculations predict that the voids in the corner near the distributor eventually fill in due to numerical error, since the bubble size is less than the level set length scale and we are using a diffuse interface method. The larger void at the vent area never fills in as the viscous gas phase gets trapped away from the vent by the paste. For the numerical solutions it is hard to make any predictions about void size, though we can say that the lower bubbles are smaller than the upper ones, and that for similar values of the dimensionless time the voids for 4B will be smaller than 4A, with 4C being somewhere in between, which does follow the experimental trend.

Next we experimented with the orientation of the mold. Molds were turned so that the distributor was perpendicular to gravity on the lower surface and the vent was moved to be on the upper surface. Results showed that orientation with respect to gravity had a large impact on the likelihood of voids remaining in the corners of the mold.

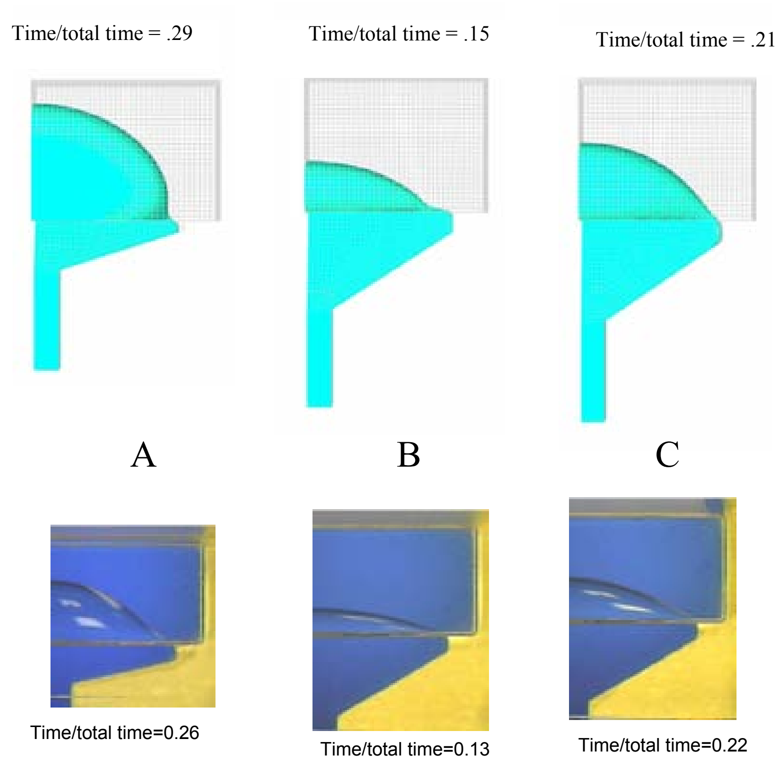

Figure 30. Comparison of the effect of distributor geometry on the shape of the fluid front entering the mold for horizontal orientation of Geometries 4A-C. Gravity is into the page.

Figure 30 shows representative video frames compared to numerical predictions just as the distributor was completely filled in a horizontal orientation of the mold. Because the fill rates varied, the time again is shown in a nondimensional form. The time it took to completely fill the original geometry 4A in the horizontal position was 23.3 ± 0.9 s, to fill the geometry of 4B was 28.9 ± 1.5 s, and to fill the geometry of 4C was 27.3 ± 1.8 s.

The top views of the horizontal orientation show that the liquid wets the top later than the bottom. It is interesting to note that the horizontal alignment causes the front to hit the far wall before even wetting the sides at all. In other words the front was less “flat” entering the mold from the distributor. This is also predicted by the numerical simulations. Again both experiments and simulations show that 4B has the flattest profile; however it is flatter in the experiments than the simulations. The time that it takes to completely fill the distributor are also showing the correct trends but do not match quantitatively.

The laboratory results also show that the horizontal orientation, with the vent on top and the distributor entrance on bottom, resulted in significantly less air trapped in the mold. When oriented vertically, bubbles are trapped in corners both opposite the distributor and opposite the vent. In the horizontal orientation the experiments result in air only being in the corners nearest the distributor. The simulations show bubbles in corners both near and far from the distributor; however the bubbles far from the distributor are both much smaller than in the vertical case and smaller than those near the distributor. Figure 31 shows the results for the horizontal and vertical orientations of Geometry 4A.

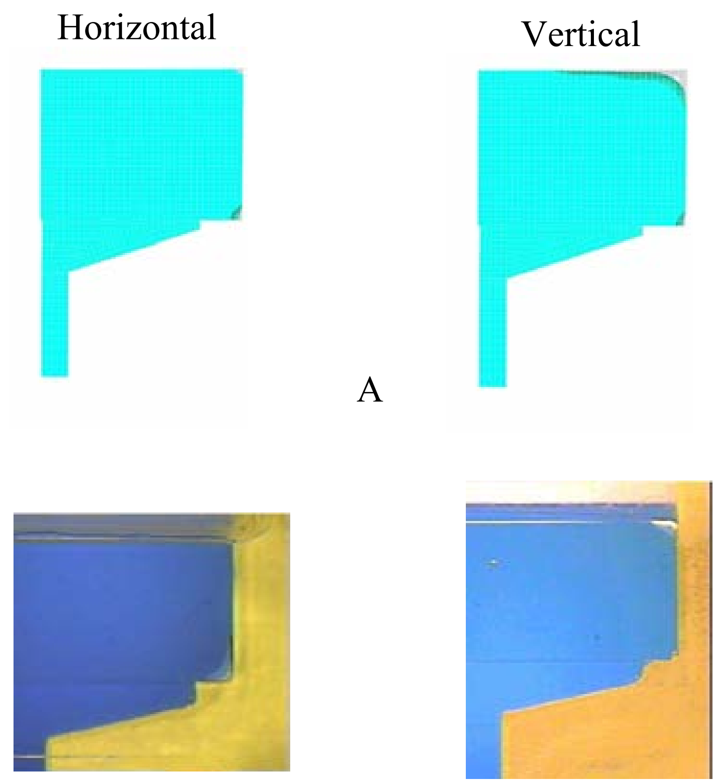

Figure 31. Simulation (above) and experiment (below) show that a vertical orientation results in trapping more air.

5.4 Geometry 2: Kansas City Boxes Revisited

Geometry 2, used in the earlier sensitivity studies as a 2D geometry, represents a simplified geometry that mimics aspects of Kansas City encapsulation processes. This geometry again involves flow into a mold, but this time the liquid must flow around obstacles, which could represent wires or other electronic components. The domain represents the interior of a rectangular cavity. Four cylindrical posts act as obstructions within the cavity.

In the actual laboratory version, the dimensions of the box are as follows: length = 1.735 cm, width = 1.735 cm, height = 1.306 cm. A typical diameter for the cylindrical posts is 0.508 cm. They are positioned on 0.578 cm centers. UCON 95-H-90000 or UCON 95-H-9500 is injected into the cavity from a circular gate (diameter = 0.312 cm) positioned at the center of one of the lateral faces of the box for Geometry 2A and positioned at a corner (the box is rotated so that this corner is the lowest point) for Geometry 2B. Figure 32 shows photographs of the laboratory apparatuses made from a stereolithography process with the material DSM Somos 12120. The experimental procedure was the same as that described above for Geometry 4.

A B

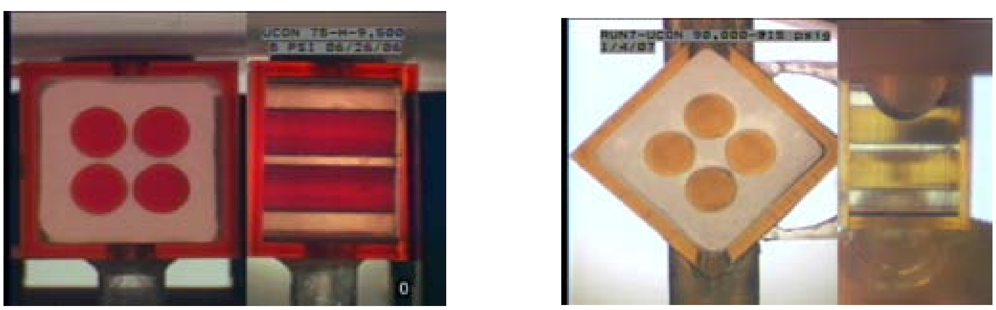

Figure 32. Apparatus from front and side for geometry 2A and 2B.

We first compared the experimental results using UCON 95-H-90000 to the results of the sensitivity study done earlier with estimated properties. Although the wetting parameters used in the calculations varied from the experimental ones, the *Ca* and *Re* were in both cases about 20 and 0.001, respectively. The wetting speed for the real liquid was measured, as mentioned above, to be 0.0013cm/s, but the sensitivity study used a wetting speed of 1 cm/s. An inflow velocity boundary condition was used that resulted in in a fill time of 5 s for the simulation whereas the experiment had a fill time of 12 s. Despite the differences in properties, Figure 33 shows that the results are surprisingly similar if viewed at the same nondimensional time (t* = time/total time).

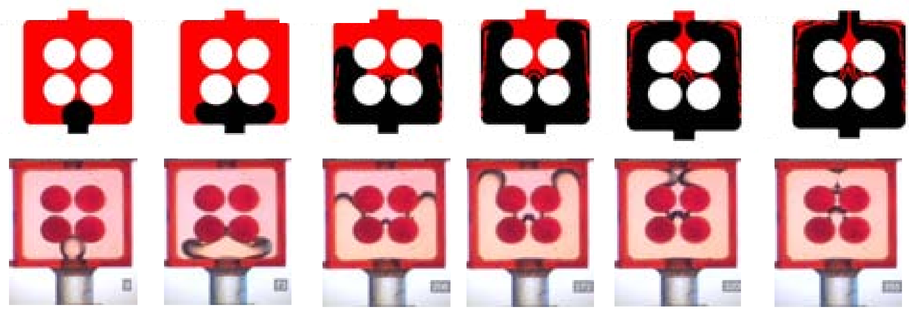

t*=0.03 t*=0.2 t*=0.6 t*=0.8 t*=0.9 t*=1.0

Figure 33. Comparison of earlier sensitivity study 2D numerical calculations (top) to experimental results (bottom) in geometry 2A.

New 2D simulations were performed for geometry 2B with the inlet at the corner using ARIA. Properties used are those of UCON 95-H-90000 wetting DSM Somos 12120, as listed in Table 7.

Table 7. Properties used in calculations for Geometry 2.

Material Property	**Value**
Density of liquid	1.09 g/cm^3
Viscosity of liquid	390 Poise
Density of gas	0.0011 g/cm^3
Viscosity of gas	0.39 Poise
Wetting speed, v_o	0.00193 cm/s
Blake scale factor, γ	2.01
Static contact angle	39.8^o
Surface tension	40 dyne/cm

Figure 34 shows results both of the simulations and the experiment for geometry 2B. Changing the injection location does change the flow path but a bubble still forms between the posts. In the experiment the bubble will eventually break in two and float around the top post if the flow continues to overfill the box. Some of the gas escapes but not all. The escape seems unpredictable and irreproducible. In the simulations the slower wetting speed measured for the oil prevents the posts from wetting quickly enough, and a larger bubble is left as the liquid begins to exit. However, the general nature of the flow and bubble formation is captured. Increasing the wetting speed results in a better match with experiment.

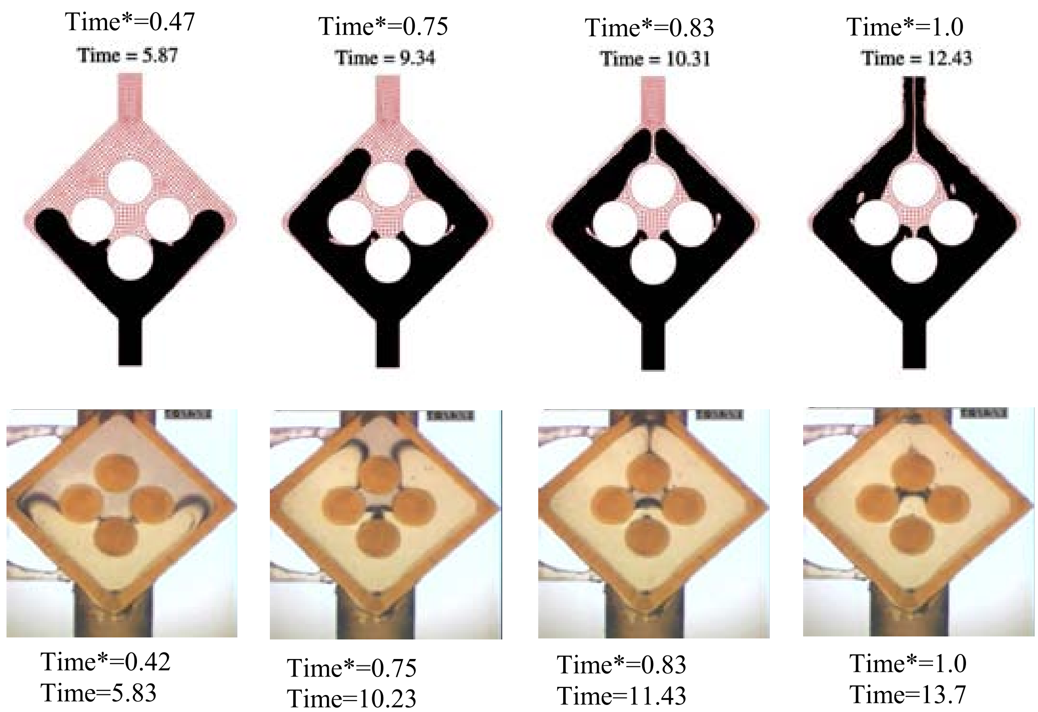

Figure 34. Comparison of 2D simulation (top) to experimental data in geometry 2B. Time* is the time normalized by the time it takes for the liquid to first exit the tube at the top of the mold.

Figure 35 shows that the simulations differ little if the flow rate is halved. Again the calculations are for UCON 95-H-90000.

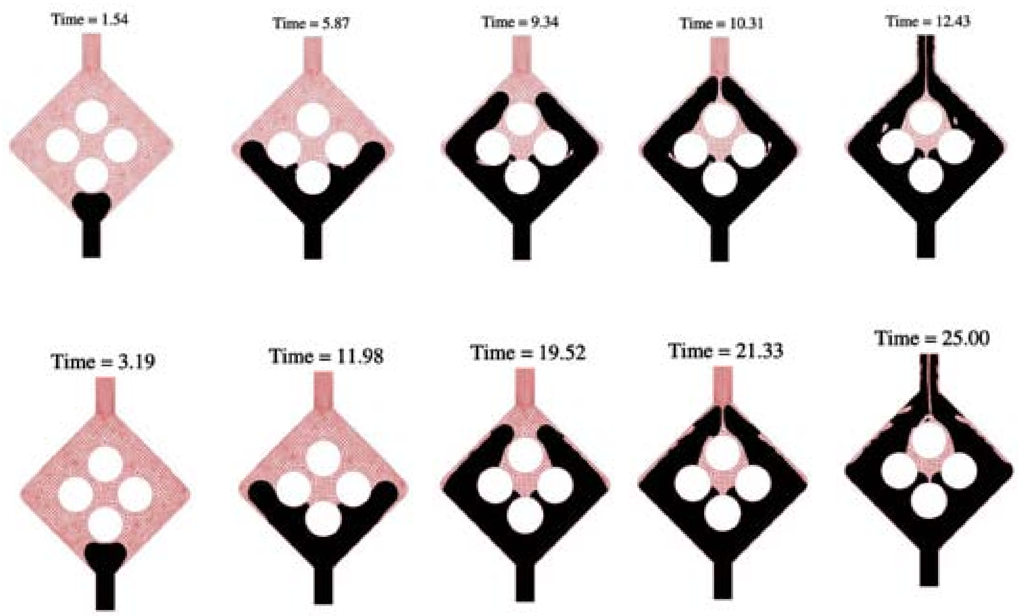

Figure 35. Comparison of simulations with a fill time of about 12.4 s and with a flow about half as fast. Liquid has properties of UCON 75-H-90000.

Three dimensional simulations were performed for geometry 2A using ARIA. Properties used are those of UCON 95-H-90000 wetting DSM Somos 12120, again as listed in Table 7.

Figure 36 shows that the simulations again match well with the experiments, although the wetting between posts still lag the experiment. Increasing the number of elements somewhat in this area did not influence the results. The 3D simulations did, however, clearly show that the bubbles left near the exit were only on the front and back walls, as shown in Figure 37.

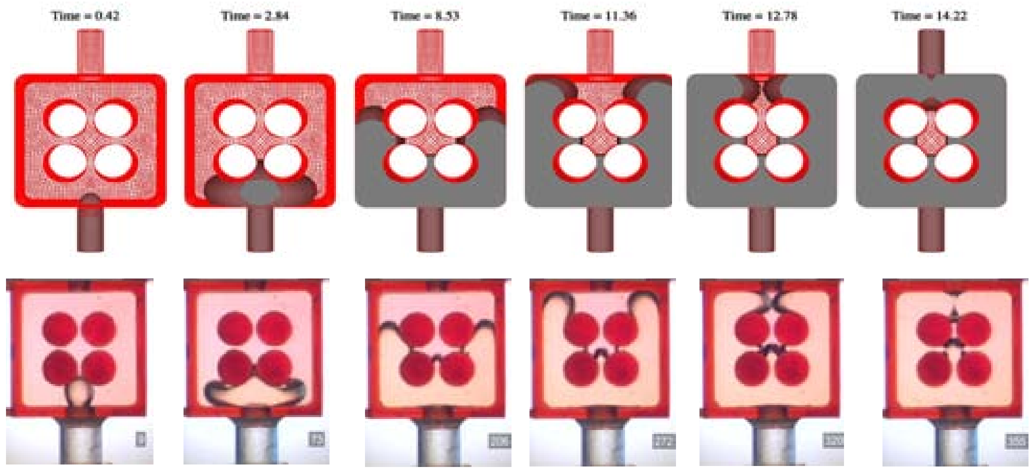

Figure 36. Comparison of 3D ARIA calculation (top) in geometry 2A to experimental results (bottom) at comparable relative times. The depiction of the mesh disappears when the front surface is wetted in the calculations. In the experiment it is more difficult to tell where the front surface is wetted, but the dark areas are clearly away from the front wall.

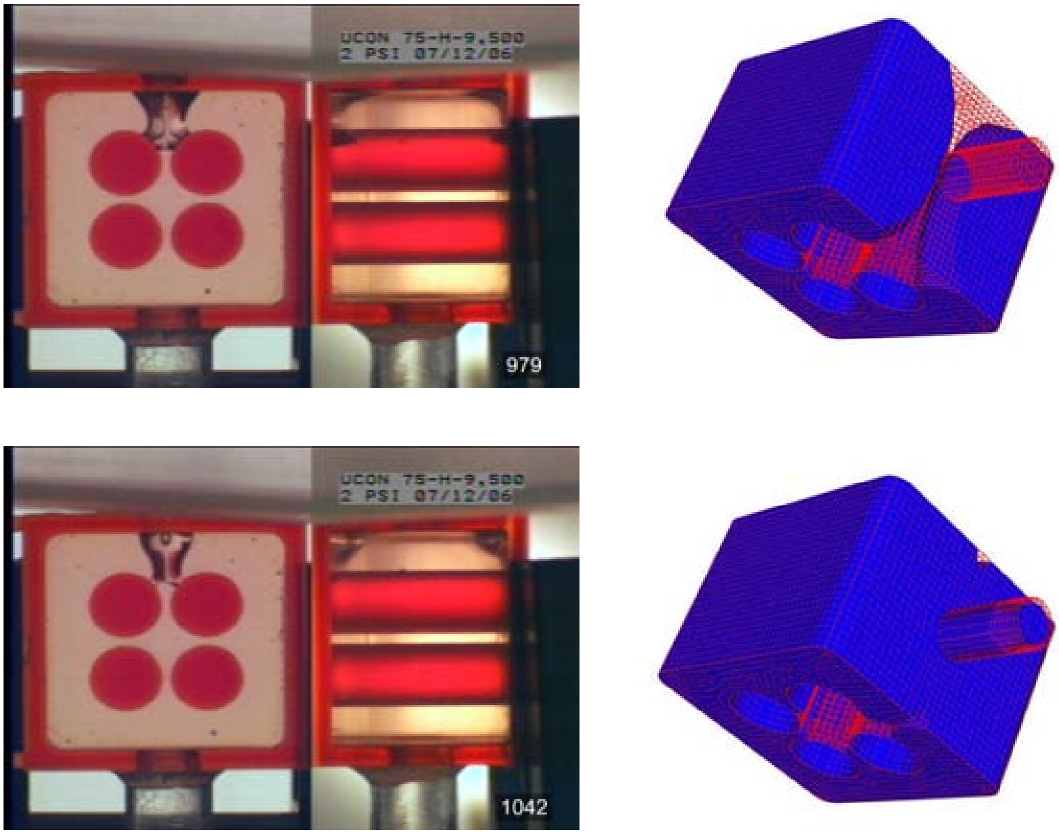

Figure 37. 3D ARIA calculation correctly shows bubbles left at exit near walls. Left, views of the experiment (left from front, right from side) as liquid knit lines meet and as liquid begins to leave the top. Right, corresponding frames from simulation.

6. Results of ProCAST Simulations

The flow of material into Geometry 2A was also modeled in 3D using ProCAST. The 3D flow domain illustrated in Figure 38 is comprised of 23369 nodes and 19488 8-node, tri-linear, hex elements. Properties of the filling liquid for this sample problem are noted: density = 1.091 g/cm^3, viscosity = 47 Poise, surface tension = 37 dynes/cm. These properties were taken to be close to those of the RSF200 encapsulation material as well as the UCON 95-H-90000. No slip boundary conditions were prescribed on the velocity field for all confining walls of the domain. A uniform velocity of 3.75 cm/s was imposed at the circular inlet. Atmospheric pressure equal to 12.2 psi was maintained at a corresponding circular outlet (located opposite the inlet port on the backside lateral face of the cavity).

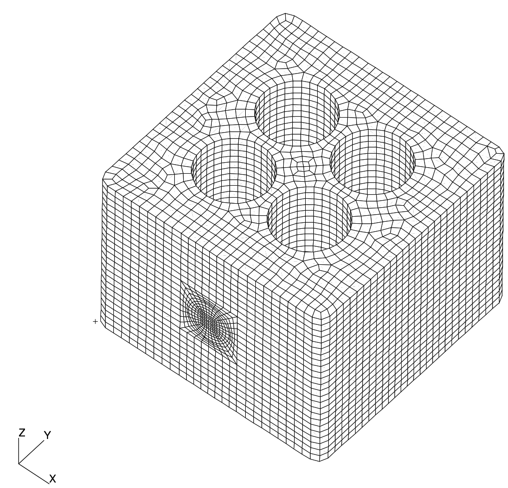

Figure 38. Mesh used for ProCAST calculations.

Figure 39 shows snapshots of at various times during the filling of the cavity. Although not shown, the cavity eventually fills completely because of the inlet condition that was prescribed: uniform velocity (mass flux) at the inlet. Fill time was recorded to be 20.04 seconds which required 19 minutes on a 2.8GHz, Intel-Xeon HP-workstation.

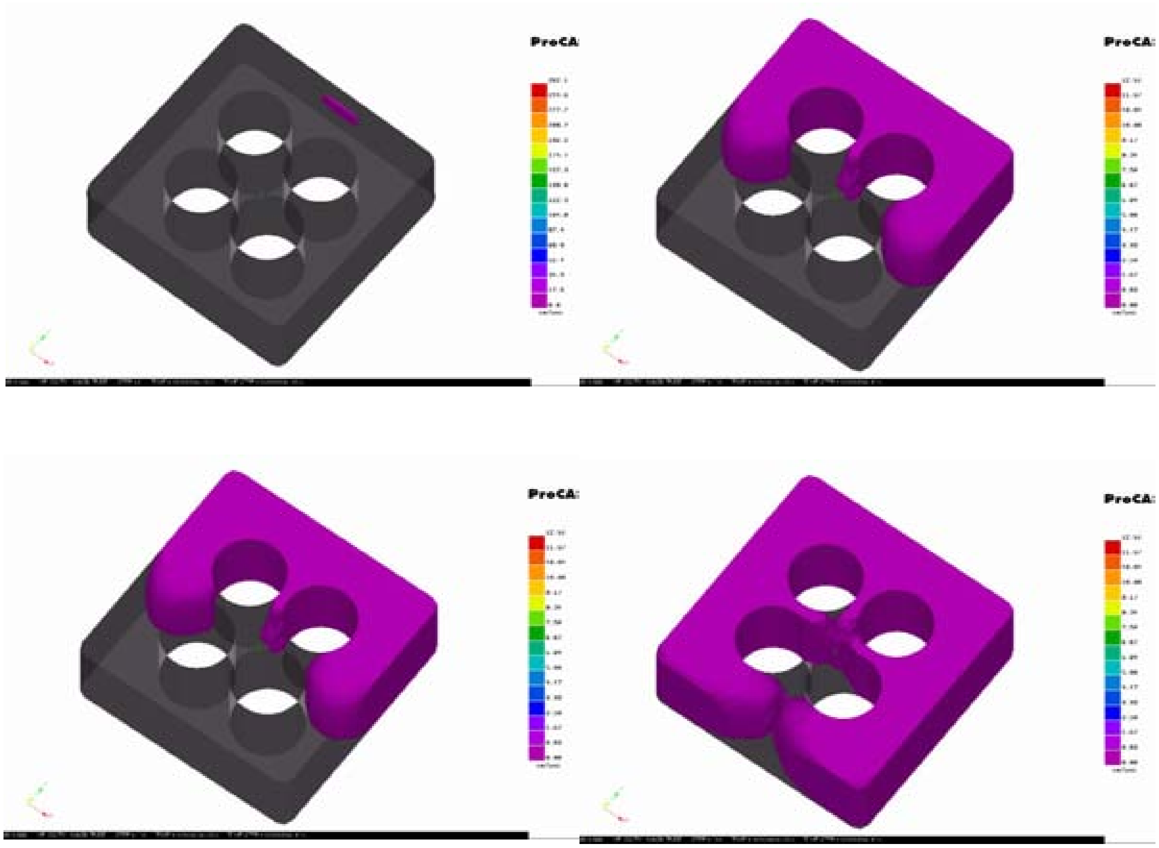

Figure 39. ProCAST simulation. Although the simulation predicts that the cavity will fill completely, snapshots before this indicate correctly the last areas to fill, which in turn represent bubble formation.

Figure 40 illustrates an alternative filling simulation which features a trapped-gas model. In this instance, a pressure of 12.31 psi is specified at the cavity inlet. This boundary condition is different than that for the case of constant mass flux, especially in conjunction with the trapped-gas model. With this problem configuration the filling fluid will respond to the presence of trapped gas, which offers resistance to further filling. Indeed this is evident in the results shown in Figure 40 – this snapshot depicts the final fill state for this particular simulation. Because of the filling transient, a trapped air pocket forms between the four interior posts, pressure builds and prevents the liquid from completely filling the cavity (at this level for the inlet over-pressure of 0.11 psi). The results are very similar to the 3D ARIA results (Figure 37) despite having no sophisticated wetting models. However, the sizes of the bubbles near the exit are smaller than predicted by ARIA and smaller than observed in the laboratory.

Simulation time for this filling sequence was 12.34 seconds. Computer run time was 11 minutes on the same hardware, which is considerably faster than the comparable ARIA calculations.

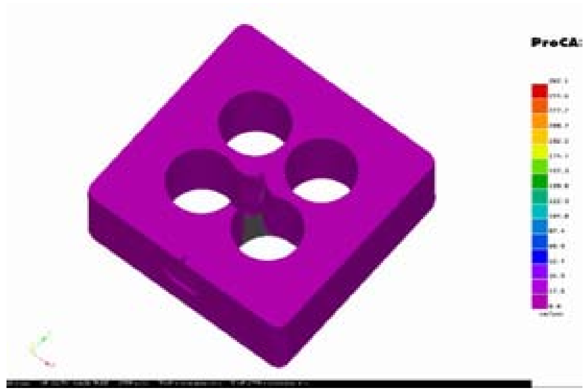

Figure 40. ProCAST prediction of the completed fill using a trapped-gas model.

7. Results of MOLDFLOW Simulations

Preliminary evaluations of MOLDFLOW were also conducted, which focused on strictly isothermal viscous flow through 3D cavities. Here we will report on the same Geometry 2A. The mesh was composed of linear tetrahedron elements, based on the existing 3D CAD part model.

Figure 41 shows the filling sequence. Comparison with the experimental snapshots shows that MOLDFLOW captures the essential flow behavior. However, like ProCAST without the trapped-gas model, MOLDFLOW will always predict a complete fill. Therefore, one looks at the last areas to fill as likely locations to trap gas. In addition, MOLDFLOW has the capability to constantly review flow separation and closure across regions. Figure 42 indicates where air traps may be present due to this phenomena. The green markers in the plot indicate where air might be present, or in some cases, where air was trapped and later moved due to the flow path. In this example, no gravity is present so there is high evidence of flow regions separating and trapping air in the box as the flow closes off the exit hole (noted on the top of the box).

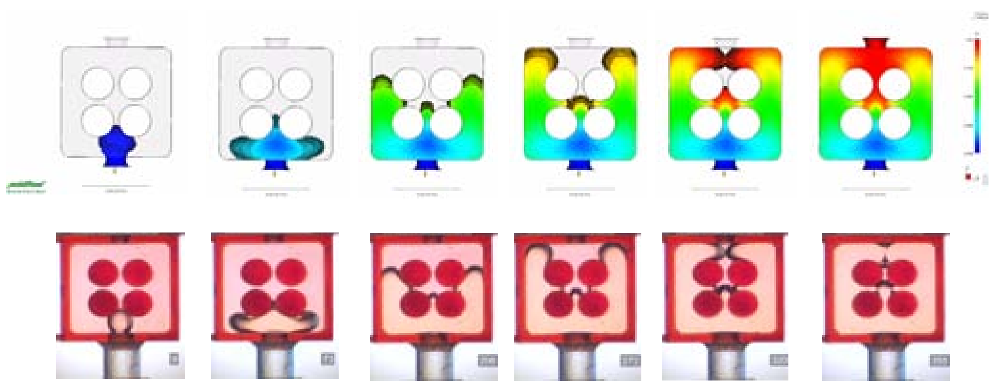

Figure 41. MOLDFLOW results compared to the experiment (Figures 33 and 36). Colors represent time to reach that point. Red areas would be the last to fill and could represent void locations.

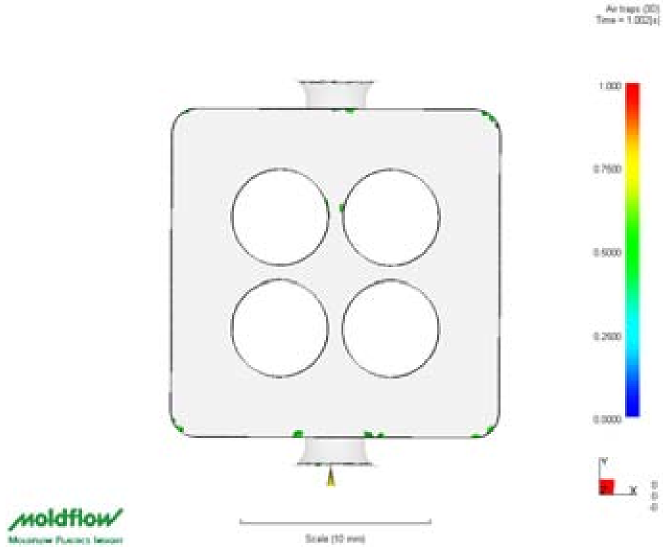

Figure 42. Gas traps predicted by MOLDFLOW indicated in green for a fill time of 1 second.

Figure 43 illustrates that, when the flow rate is drastically reduced by a factor of 100, the predicted behavior is very different and could result in far less trapped air. Although lowering the flow rate by this amount for a pressure-driven fill from the bottom was not possible with our existing laboratory apparatus, we did see indications that trapped air could be dramatically lowered with an extremely slow fill when we allowed a less viscous (by a factor of 10) liquid drip slowly from the top of the box (Figure 44). Here, the fluid front rose with a much flatter shape resulting in no trapped bubble between the posts.

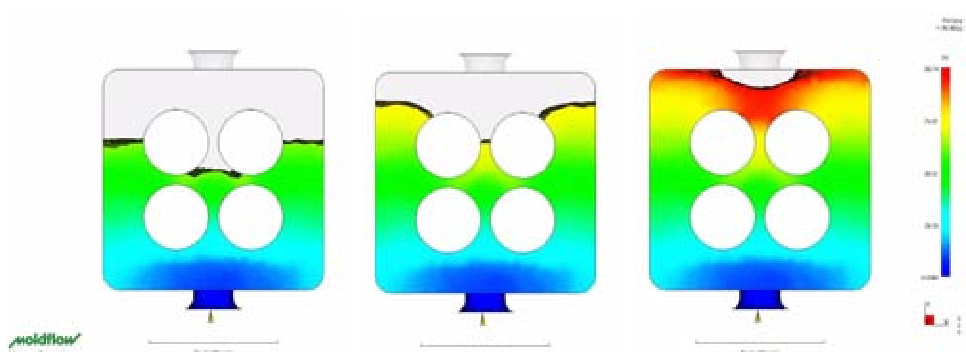

Figure 43. MOLDFLOW predictions with a fill time 100 times longer than in Figure 41.

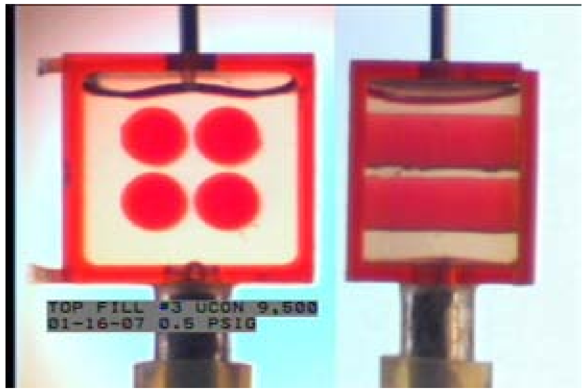

Figure 44. Snapshot of the fill process when liquid drips slowly from the top of the box, showing a flatter profile and no bubbles trapped between the posts.

8. Conclusions

As part of an effort to reduce costs and improve quality control in encapsulation and potting processes the Technology Initiative Project "Defect Free Manufacturing and Assembly" completed a computational modeling study of flows representative of those seen in these processes. Flow solutions were obtained using a coupled, finite-element based, Newton-Raphson numerical method based on the GOMA/ARIA suite of Sandia flow solvers, which include an advanced imbedded interface method to follow a moving boundary and advanced dynamic wetting models. In addition, two commercially available codes, ProCAST and MOLDFLOW, were also used on geometries representing encapsulation processes at the Kansas City Plant. ProCAST has the capability to include gas pressure which allows a more realistic trapped gas model, but both can give valuable information about the fill process and areas that are likely to trap gas.

Visual observations of the flow front in several geometries were recorded in the laboratory and compared to the models. Wetting properties for the materials in these experiments were measured using a unique flow-through goniometer, in which a droplet is observed and recorded as it spreads on a solid surface.

Both 2D and 3D models were examined. Results show that two dimensional modeling can often show qualitative trends, such as regions that are likely to trap bubbles, even if the quantitative values of bubble size are not exact. Although requiring more time and resources, 3D models can improve the quantitative predictions.

Modeling with GOMA/ARIA captured many of the trends of the experiments, though quantitative agreement is often lacking. We feel that the lack of agreement between the experiment and simulation probably stems from several factors, including the diffuse interface representation in the level set algorithm, as well as the assumed high value for the gas phase viscosity necessary for numerical stability.

Simulations of bubble spreading with GOMA showed that the finite thickness of the interface that must be assumed in the model increased the resulting contact angle. In order to match the experiment, input parameters must be changed to reflect this. Our experience leads us to believe that increasing the parameter v_o in the Blake (1993) model (equation 2) is a good way to accomplish this. Dynamic wetting is a molecular-scale event in reality, and these models for incorporation into a continuum-scale calculation must reflect the molecular physics in a grossly simplified way. Furthermore, the parameters for this continuum-scale model are not necessarily material properties, but could actually depend on the flow itself. Wetting is currently a research topic, and this work may indicate that parameters determined in one flow field do not necessarily hold for all flows. Since dynamic wetting is still a research topic, understanding the best way to estimate this process will require more experiments and code validation runs that are not in the scope of the present work. Nevertheless, we have shown through a sensitivity study that flow over an indentation requires sophisticated wetting models to capture the subtleties that may be important in a manufacturing process. In addition, similar aspects in other flows, such as the details of bubbles trapped in corners for example, are better represented with the more sophisticated wetting models.

Similarly, the artificially high gas viscosity especially affects flows in which fluid must displace gas in a cavity (Figures 28-31). In contrast, results in flow over an indentation showed little effect of increasing the gas viscosity (Figures 21-24). If the problem allows this to be done without adverse effects, the computational time requirements can be reduced.

For geometries in which the liquid must flow around obstacles, the likelihood of trapping bubbles between the obstacles is relatively insensitive to the wetting properties (Figures 33-41). Although the wetting is important in showing the evolution of the bubble from capture between the posts to partial escape with the flow and gravity. When the parameter v_o was set to an extremely high value in the sensitivity study (before measurements were actually available) the fluid in the simulations could push through the posts and displace some of the trapped air as seen in the experiments (Figure 33). Deattachment of bubbles is yet another difficult phenomena to understand and capture at a continuum-scale and again will require more study to better predict the behavior. Nevertheless, if one only wants information about the initial locations of trapped gas, commercial codes with more simplified approximations to the physics also are shown to be able to give valuable information about the process.

In the case of the Kansas City encapsulation processes, even simple modeling can also give valuable information about the volume of material needed to fill the part. Although this may be easy to calculate for the simple box example shown in this report, a value for a real part with complex geometry is never known until late in the production process. It is not uncommon to get electronic sections to have surface counts on the order of 1000 - 2000. Current methods for this volume determination is done using the liquid volume method with alcohol and mock parts.

The best way to gain insight into the filling patterns shown in this report, of course, is to view videos of the simulation sequences and videos of the laboratory processes. Unfortunately, this format was cumbersome to include in the written document. Nevertheless, these simulation tools include post-processing capabilities to produce movies that can be very powerful for flow visualization to add understanding to encapsulation and potting procedures that are generally not observable in actual practice.

In summary, we believe that the major lessons learned from this work include:

- *Modeling and simulation can help determine the important phenomena* in areas of concern. For example, the initial trapping of bubbles in flow of highly viscous liquids around obstacles is relatively insensitive to wetting properties, whereas the filling of a cavity or indentation is more sensitive to wetting.

- *Modeling and simulation should be used early to aid in the design process.* In extremely complex geometries modeling can review the overall volume necessary for the fill and aid in determining areas where gates should be placed. Effect of timing of the flow can also be examined.

- *Bubbles formed from flows can be most easily mitigated by reducing the flow rate.* This is especially true in flow over indentations. Lowering the viscosity and increasing the wetting of the material can also help, but often these are less easily varied in a process. *Drastically* reducing the viscosity and flow rate can also help prevent bubbles from forming in the flow around obstacles by reducing the propensity of the front to bulge and trap air in knit lines. However, this is not within the range of possible variations in some encapsulation materials because of the cure pot-life and because many are loaded with solid particles to achieve necessary final properties and so are highly viscous.

- *It may not be possible to eliminate bubbles formed in flows where liquid displaces gas in complex cavities filled with multiple obstacles* within the range of parameters possible. Vacuum processing would offer a viable alternative.

We recommend the use of MOLDFLOW, ProCAST, and GOMA/ARIA based on validation experiments. Of course all modeling should be done with the awareness of the codes' inherent limitations. MOLDFLOW should be limited to initial reviews and to materials with low surface tensions. ProCAST can be used likewise, and with the use of the trapped-gas capabilities it can also provide better estimates of the volume of bubbles likely. GOMA/ARIA can be used with a wider range of materials and for problems with more sensitivity to wetting issues. Although not explored in this report, encapsulation and potting materials are curing, with time and temperature dependent viscosities and limited pot life. Any modeling done should adequately account for these changes in properties.

9. References

Baer, T.A., D.R. Noble, R.R. Rao, and A.M. Grillet, “A Level Set Approach to 3D Mold Filling of Newtonian Fluids,” Proceedings of the ASME Symposium on Flows in Manufacturing Processes, Honolulu, Hawaii, July 6-10, 2003.

Berchtold, Kathryn, personal communication, Los Alamos National Laboratory (2006).

Bird, R.B., R. C. Armstrong, and O. Hassager, *Dynamics of Polymeric Liquids*, Wiley, New York, New York (1987).

Blake, T.D. and J.M. Haynes, “Kinetics of liquid/liquid displacement ,” J. Colloid Interface Sci., 30, 421 (1969).

Blake, T.D. “Dynamic contact angles and wetting kinetics,” Wettability, John C. Berg, ed. Marcel Dekker (1993).

Blake, T.D. and J. De Coninck, “The influence of solid-liquid interactions on dynamic wetting,” Advances in Colloid and Interface Science, 96, 21-36, 2002.

Brooks, C. F., A. M. Grillet, and J. A. Emerson, “Experimental investigation of the spontaneous wetting of polymers and polymer blends,” Langmuir, 22, 9928-9941 (2006).

Dohrmann, C. R. and P.B. Bochev, “A stabilized finite elements method for the Stokes problem based on polynomial pressure projections,” International Journal for Numerical Methods in Fluids, 46, 183 (2004).

Ferguson, J. and Z. Kemblowski, *Applied Fluid Rheology*, Elsevier Applied Science, New York, pp. 52-55, (1991).

Jacqmin, D., “Three-dimensional computations of droplet collisions, coalescence, and droplet/wall interaction using a continuum surface-tension method,” AIAA-95-0833.

Notz, P.K, S.R. Subia, M.M. Hopkins, D.R. Noble, H.K. Moffat, D. Neckles, http://aria.sandia.gov/.

Probstein, Ronald F. Physicochemical Hydrodynamics, 2nd Ed., John Wiley & Sons, New York, pp 305-361 (1994).

Rao, R. R., L. A. Mondy, P. R. Schunk, P. A. Sackinger, D. B. Adolf, “Verification and Validation of Encapsulation Flow Models in GOMA, Version 1.1,” Sandia National Laboratories, SAND2001-2947, October 2001.

Reddy, S., P. R. Schunk, and R. T. Bonnecaze, “Dynamics of low capillary number interfaces moving through sharp features,” *Physics of Fluids* **17**, 122104-1 – 122104-6 (2005).

Rutherford, Brian, personal communication, Sandia National Laboratories (2005).

Sethian, J.A., *Level Set Methods and Fast Marching Methods*, Cambridge University Press, (1999).

Sartor, L., Slot Coating: Fluid Mechanics and Die Design, University of Minnesota, Ph.D. Thesis, (1990).

Schunk, P.R., P.A. Sackinger, R.R. Rao, K.S. Chen, T.A. Baer, D.A. Labreche, A.C. Sun, M.M. Hopkins, S.R. Subia, H.K. Moffat, R.B. Secor, R.A. Roach, E.D. Wilkes, D.R. Noble, P.L. Hopkins, and P.K. Notz, "GOMA 4.0 – A Full-Newton Finite Element Program for Free and Moving Boundary Problems with Coupled Fluid/Solid Momentum, Energy, Mass, and Chemical Species Transport: User's Guide," Sandia National Laboratories, SAND2002-3204, October, 2002.

Sun, A.C., T.A.Baer, S. Reddy, L.A. Mondy, P. R. Schunk, P.A. Sackinger, R. R. Rao, D.R. Noble, J. Bielenberg, and A. Graham, "Wetting in pressure driven slot flow," Moving Boundaries 2005, Eighth International Conference on Computational Modelling and Experimental Measurements of Free and Moving Boundary Problems, La Coruna, Spain, September 21-23, 2005.

William, M.L., R.F. Landel, and J.D. Ferry, "The Temperature Dependence of Relaxation Mechanisms in Amorphous Polymers and Other Glass-Forming liquids," J. Am. Chem. Soc., 77, 3701 (1955).

Young, T. "An essay on the cohesion of fluids." Philos. Trans. R. Soc. London 95, 65-87 (1805).

Distribution:

1	MS0384	Art Ratzel	1500
1	MS0825	Michael Prairie	1510
1	MS0834	Robert Tachau	1512
1	MS0834	Jaime N. Castañeda	1512
1	MS0834	Ray Cote	1512
1	MS0834	Carlton Brooks	1512
1	MS0834	Anne Grillet	1513
1	MS0826	Dan Rader	1513
1	MS0836	Andrew Kraynik	1514
1	MS0836	Rick Givler	1514
1	MS0836	Matt Hopkins	1514
1	MS0836	Joel Lash	1514
10	MS0836	Lisa Mondy	1514
1	MS0836	David Noble	1514
1	MS0836	Pat Notz	1514
5	MS0836	Rekha Rao	1514
1	MS0836	Edward Wilkes	1514
1	MS0380	Hal Morgan	1540
1	MS0382	Steve Gianoulakis	1541
1	MS0888	Doug Adolf	1821
1	MS0886	James Aubert	1821
1	MS0319	Marc Polosky	2614
1	MS1064	Allen Roach	2614
1	MS0501	Sarah Leming	5343

2	MS9018	Central Technical Files	8944
2	MS0899	Technical Library	4536